DESIGN OF A 60 GHz, 100 kW CW GYROTRON FOR PLASMA DIAGNOSTICS

A DISSERTATION

Submitted in partial fulfillment of the requirements for the award of the degree of

MASTER OF TECHNOLOGY

in

ELECTRONICS AND COMMUNICATION ENGINEERING

(With Specialization in RF and Microwave Engineering)

By

RAGINI JAIN

M.G. CENTRAL LIBRARY
ACC No. G20077
Date 20/10/10
I.I.T. ROORKEE

DEPARTMENT OF ELECTRONICS AND COMPUTER ENGINEERING
INDIAN INSTITUTE OF TECHNOLOGY ROORKEE
ROORKEE -247 667 (INDIA)

JUNE, 2010

CANDIDATE'S DECLARATION

I hereby declare that the work being presented in the dissertation entitled, "***Design of a 60 GHz, 100 kW CW Gyrotron for Plasma Diagnostics***" in partial fulfillment of the requirements for the award of the degree of ***Master of Technology*** in ***Electronics & Communication Engineering***, submitted in the Department of Electronics and Computer Engineering, Indian Institute of Technology Roorkee (India), is an authentic record of my own work carried out under the guidance of Dr. M.V. Kartikeyan, Professor, Department of Electronics & Computer Engineering, Indian Institute of Technology Roorkee.

The matter embodied in the dissertation report has not been submitted for the award of any other degree elsewhere.

Date : 14-06-10
Place : IIT Roorkee

Ragini Jain.
(Ragini Jain)

CERTIFICATE

This is to certify that the above statement made by the candidate is correct to the best of my knowledge.

Date : 14.06.2010
Place : IIT Roorkee

Dr. M.V. Kartikeyan
Professor
E&CE Department
IIT Roorkee

ACKNOWLEDGEMENTS

It gives me great pleasure to take this opportunity to thank and express my deep sense of gratitude to my guide **Dr. M.V. Kartikeyan**, Professor, Department of Electronics and Computer Engineering, Indian Institute of Technology Roorkee, for his valuable guidance, constant motivation, patience and enthusiasm, which were immensely helpful in carrying out this work.

Special thanks to **Dr. S.N. Sinha**, Head of E&C Department, for facilitating the necessary requirements to carry out the work and for supporting at critical time during the thesis submission. I would also like to thank **Dr. D. Singh**, **Dr. A. Patnaik** and **Dr. N.P. Pathak** for their encouragement and guidance in the RF and Microwave field during the entire tenure in IIT.

I thank **Dr. Jagadish Mudiganti**, **Mr. Ashwini Arya** and **Dr. Narendra Chauhan** for their valuable support and time to time guidance in technical issues, which was instrumental in making this dissertation work a success.

My special sincere heartfelt gratitude to my family, whose sincere prayer, best wishes, support and encouragement has been a constant source of strength to me during the entire work. I also thank Bharat for the continuous encouragement and for helping me in improving the quality of this report. Finally, I would also like to thank all my friends, especially Prateek, Manasi, Shrabony, Karmugil, Rahul, Mangesh, Padmaja, Sarika and my brother Vaibhav for their support and valuable suggestions.

Ragini Jain.
(Ragini Jain)

ABSTRACT

Gyrotrons are high power microwave/millimeter wave sources capable of producing hundreds of kilowatts of long pulse to CW power. They are being used in a variety of Industrial–Scientific–Medical (ISM) applications ranging from plasma heating in thermonuclear fusion reactors to industrial heating of materials (particularly nano powders). It is basically an electron cyclotron maser (ECM) in which the electromagnetic energy is radiated by relativistic elecrons gyrating in an external longitudinal magnetic field.

In this work, the design studies of a 60 GHz, 100 kW, CW gyrotron are presented. Mode selection is carefully studied with the aim of minimizing mode competition; few operating modes are chosen which are capable of giving a perfect solid beam output through a synthetic double–disc window with a suitable dimpled–wall quasi–optical launcher. Cavity design and interaction computations are then carried out. In addition, preliminary design of the launcher, window, magnetic guidance and beam optic system are presented. Thus, a comprehensive conceptual study is presented which indicates that the operation of such a gyrotron is possible and can give power in excess of 100 kW at $> 35\%$ efficiency.

A Graphical User Interface package "GDS V.01" (Gyrotron Design Suit Ver.01) has been developed in MATLAB R2006a on HP xw6400 Workstation having 3 GB RAM. The software incorporates the mode selection procedure, starting current calculations, gun synthesis and design of coils, resonator design and RF–behavior calculations, launcher design, non–linear taper design and window design. This package can be used to carry out feasibility studies and conceptualization of specific gyrotrons.

Contents

List of Figures

List of Tables

Chapter 1

Introduction

Gyrotron oscillators (gyrotrons) are capable of providing hundreds of kilowatts of power at microwave and millimeter wavelengths. From their conception in the late fifties until their successful development for various applications, gyrotrons have come a long way technologically and made an irreversible impact on both users and developers. Gyrotron technology has significantly advanced during this time towards meeting the goals of providing a reliable and highly efficient source of high–power millimeter wave radiation.

1.1 General Introduction

The gyrotron is a source of high power coherent radiation. It consists of a magnetron injection gun, which generates an annular electron beam which is focused into an open cavity resonator along an axial magnetic field, created by a superconducting magnet. In the cavity, the RF field interacts with the cyclotron motion of the electrons in the beam and converts the transverse kinetic energy into a RF beam which may then be internally converted into a Gaussian beam. The spent electron beam leaves the cavity and propagates to the collector where it is collected.

Gyrotron systems have proven useful where conventional microwave sources have not

been adequate. This is demonstrated by the number of applications in which they can be found. The possible applications of gyrotron oscillators and other electron cyclotron masers (ECMs) / fast–wave devices span a wide range of technologies [1]:

(i) RF plasma applications for magnetic confinement fusion studies, such as

  a) electron cyclotron resonance heating and current drive (ECH/ECCD) (28–170 GHz),

  b) plasma start–up,

  c) plasma diagnostic measurements,

(ii) Deep–space and specialized satellite communication,

(iii) High–resolution Doppler radar, radar ranging and imaging in atmospheric and planetary science,

(iv) Drivers for next–generation high gradient linear accelerators,

(v) ECR ion sources,

(vi) Sub–millimeter wave and THz spectroscopy,

(vii) Materials processing, and

(viii) Plasma chemistry.

In the millimeter– and submillimeter–wavelength regions, the power that gyrotrons can radiate in continuous–wave and long–pulse regimes, exceeds the power of classical microwave tubes by many orders of magnitude. Millimeter and sub–millimeter wave plasma diagnostics are very valuable for the study of plasmas in magnetic confinement fusion experiments. Low to moderate power collective Thomson scattering provides data on instabilities, plasma waves, and turbulence. High power scattering from the ion thermal feature can provide measurements of localized ion temperature, effective Z, current density, alpha particles and D/T fuel ratios [2]. The unique features of gyrotrons are:

- High interaction efficiency (35% overall efficiency, 50% with energy recovery system)
- Single mode operation
- Availability of sources ranging from centimetric to submillimetric wavelengths
- High power (from a few watts up to 1 MW depending on pulse length) and high energy per pulse (up to 3.6 MJ at 170 GHz, 450 kW).

Thus gyrotron is considered as the best candidate for a wide spectrum of applications ranging from fusion plasma heating, profile control, current drive, and diagnostics for fusion plasmas, to industrial microwave sintering or to electron paramagnetic resonance (EPR) studies [3]. They take the advantage of a cyclotron resonance condition to transfer energy from an electron beam to an electromagnetic wave.

1.2 Motivation and Scope

Intense work on gyrotrons is being carried out for some important applications, first of all for heating of plasmas at nuclear fusion installations and high temperature processing of materials. These efforts have resulted in considerable progress in transfer from long pulses to real CW regime at the highest output power as well as in considerable increase in efficiency of gyrotrons.

The goal of the work is to see the feasibility of CW operation of a 60 GHz conventional cavity gyrotron with an output power in excess of 100 kW for plasma diagnostics in India. Plasma diagnostics in the millimeter and submillimeter wavelength range are valuable for the measurement of a wide range of plasma parameters including density, electron and ion temperatures, magnetic field direction, and non–thermal fluctuations. Gyrotrons can make an important contribution to the advancement of these diagnostics.

1.3 Related Literature Review

Substantial work on gyrotrons has been done in the development of gyrotrons for plasma diagnostics in thermonuclear fusion experiments, materials processing, technological applications and medical applications as given in [1, 4] and the references therein. CW gyrotrons at or near 60 GHz have applications for plasma heating in controlled thermonuclear fusion experiments. However, the development of 60 GHz gyrotron with a power of around 100 kW has been attempted only long ago as listed below.

For the heating of materials with smaller dielectric losses, the penetration depth is always greater. On the other hand, selective and localized heating may be possible by partially doping the materials with higher dielectric losses, which may be applicable to joining of ceramics. From these points of view, 60 GHz millimeter radiation is one of the appropriate heat sources for processing such ceramics as pure alumina as given in [5]. Here the fine focusing of millimeter–wave radiation from a high–power pulsed 60 GHz gyrotron has been performed using a two–dimensional ellipso–parabolic focusing antenna system. Millimeter waves with the cylindrical $TE_{0,2}$ mode radiated upwards from the output window of the 60 GHz gyrotron have been applied for alumina heating.

In [6], the design of a Varian 60 GHz gyrotron has been shown to generate microwave power in excess of 200 kW. The operating mode of the gyrotron was $TE_{0,2}$ with axial output collection. They used a beam velocity ratio of 2.0 with a beam voltage of 80 kV. In the pulsed mode with a pulse length of 100 msec the gyrotron could produce an output power of around 200 kW but in CW mode the maximum power achieved was 70 kW.

Machuzak [7] implemented a 60 GHz gyrotron collective Thomson Scattering alpha particle diagnostic which could launch a power of 0.1–1 kW in pulses of up to 1 sec-

ond. For this experiment, a 0.1 to 1 kW, modulated 60 GHz gyrotron was pulsed for up to 1 second into the plasma, and the scattered radiation synchronously detected.

A Varian 60 GHz, CW gyrotron was operated at power levels up to 200 kW CW [8]. The output mode of the cavity was $TE_{0,2}$ circular waveguide mode in overmoded waveguide. Since the output waveguide also served as the gyrotron collector, mode conversion occurred in the taper sections and gaps incorporated into the collector. Comparison of measurement of the mode conversion on a 60 GHz, 200 kW, 100 ms pulse tube with similar measurements on the 60 GHz, 200 kW, CW gyrotron indicated that the CW tube had significantly more conversion of the $TE_{0,2}$ mode into other modes than the pulse tube.

In all the above works, gyrotrons working with a lower order symmetric operating mode (particularly the $TE_{0,2}$ mode) with axial output collection employing an external mode converter were designed. In the present work, a comprehensive design of the 60 GHz, 100 kW, CW gyrotron with radial output collection employing an advanced dimpled–wall quasi–optical launcher has been presented. The operating mode is the $TE_{6,2}$ mode and is very well separated from other neighboring modes to avoid mode competition. An advanced dimpled–wall launcher has been used for radial output coupling, so that it can be directly used for plasma diagnostics. The exact problem statement is given in the next section and the design studies and results have been presented in the following chapters of the thesis.

1.4 Problem Statement

- To check the feasibility of CW operation of a 60 GHz conventional cavity gyrotron at a power level > 100 kW.
- The following design studies have to be performed to consolidate the design conceptualization:

  - To fix the operating mode.
  - Interaction Cavity Design.
  - Rigorous studies on RF–behavior.
  - MIG and guidance system.
  - Non–linear Taper.
  - Advanced dimpled–wall launcher.
  - RF Window.

- To develop a Graphical User Interface for the complete design procedure of a need specific gyrotron.

1.5 Organization of the Thesis

There are five chapters compiled in this dissertation including the present chapter.

- ***Chapter one*** gives a brief review of the theory and the motivation and scope on "*Design of a 60 GHz, 100 kW CW Gyrotron for Plasma Diagnostics*".
- ***Chapter two*** presents the literature survey of gyrotron theory. The principle of gyrotron is given along with the description of the various components of the device. The theory of the various procedures undertaken for the analysis of a gyrotron is also given.
- ***Chapter three*** describes the Graphical User Interface package proposed for the design of gyrotron in detail.
- ***Chapter four*** deals with the design studies of the specific 60 GHz gyrotron taken up for this dissertation. The results of all the procedures have been given.
- ***Chapter five*** concludes the thesis with the concluding remarks and outline direction for future scope.

Chapter 2

Gyrotron Theory

A brief review of the principles and theory of gyrotron and its components will be given here. A more complete and detailed description can be found in [4], [9]- [12]. This chapter presents some of the more immediately useful gyrotron equations, most importantly including a discussion of the mechanism through which the electron beam couples with the RF field and transfers its energy to the resonant cavity mode.

2.1 Principle of Operation

The arrangement of a simple gyrotron is shown in Fig. 2.1. Here, a magnetron–type electron gun is shown on the left. The voltage applied to the anode creates the electric field at the cathode. This field has both the perpendicular and parallel components with respect to the lines of the magnetic field produced by a solenoid. Thus, electrons emitted from the cathode acquire both the orbital and axial velocity components. Then, the electrons move towards the cavity in the growing magnetic field, in which the electron flow undergoes the adiabatic compression and the electron orbital momentum increases. In the region of the uniform magnetic field, the electrons interact with the eigenmode of the cavity and transform a part of their kinetic energy into microwave energy. Then, the spent beam exits from the axially

open cavity, undergoes decompression in the decreasing magnetic field and settles on the collector. The latter also functions as an oversized output waveguide in the axial output couplers. The RF output power in the TE_{mn} mode is coupled through the axial output vacuum window. While in the case of radial output coupling, a quasi-optical mode converter is connected to the output waveguide and it transforms the rotating TE_{mn} mode with axial power flow to a Gaussian mode with a radial power flow. The power is then transmitted through a radially located vacuum window as shown in Fig. 2.1.

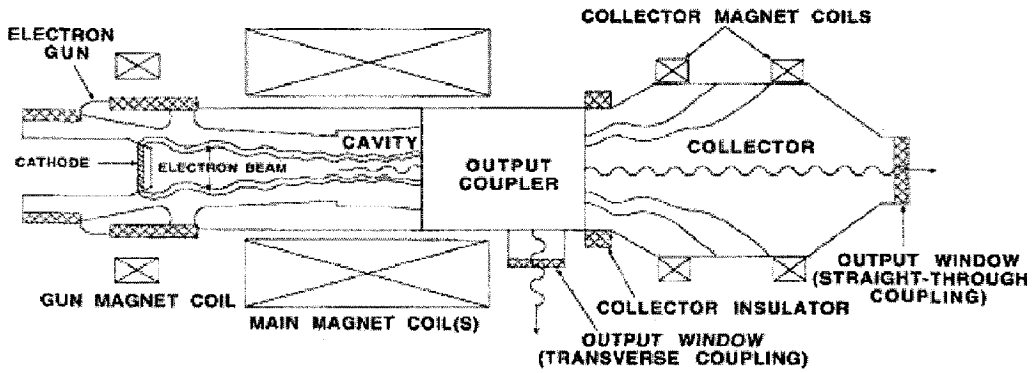

Figure 2.1: Schematic of a gyro–oscillator [9].

Classical microwave tubes require interaction structures smaller than a wavelength due to the kind of electron coherent radiation involved. Gyrotrons however, are based on the mechanism of coherent cyclotron radiation from electrons gyrating in a constant magnetic field. In these devices, the electrons can resonantly interact with fast waves, which can propagate even in free space. Therefore, the interaction space in gyrotrons can be much larger than in classical microwave tubes operating at the same wavelength. In such circuits the phase velocity v_{ph} of the EM wave is greater than the speed of light c.

The benefits of gyrodevices are derived from the combination of the cyclotron res-

onance interaction and the fast–wave interaction circuit. The electric field strength can be quite high in fast–wave devices, independent of the proximity of the metallic circuit structure. This enables the electron beam to be situated in regions of high electric field, (to produce optimum coupling) without placing the beam in close proximity to delicate circuit structures [9].

In fast–wave devices electrons undergo oscillations transverse to the direction of beam motion by the action of an external force (field) and hence they radiate. The contributions from the electrons reinforce the original emitted radiation in the oscillator or the incident EM wave in the amplifier. This is the condition of coherent radiation, which is satisfied if a bunching mechanism exists to create electron density variations of a size comparable to the wavelength of the imposed EM wave. To achieve such a mechanism, a resonance condition must be satisfied between the periodic motion of the electrons and the EM wave in the interaction region [13]:

$$\omega - k_z v_z \cong s\Omega, s = 1, 2, ...(k_z v_z = Doppler\ term) \tag{2.1}$$

Here ω is the wave angular frequency, k_z is the characteristic axial wave number, v_z is the translational electron drift velocity, Ω is an effective frequency, which is associated with macroscopic oscillatory motion of the electrons, and s is the harmonic number.

In electron cyclotron masers (ECMs), EM energy is radiated by relativistic electrons gyrating in an external longitudinal magnetic field. In this case, the effective frequency Ω corresponds to the relativistic electron cyclotron frequency

$$\Omega_c = \Omega_{co}/\gamma \ \ where \ \ \Omega_{co} = eB_o/m_o \ \ and \ \ \gamma = [1 - (v/c)^2]^{-1/2} \tag{2.2}$$

where γ is the relativistic factor. A group of relativistic electrons gyrating in a strong magnetic field will radiate coherently due to bunching caused by the relativistic mass dependence of their gyration frequency [14].

The transverse velocity component of electrons spiraling in the presence of an applied magnetic field interacts with the transverse electric (TE) modes of a simple waveguide or cavity circuit structure. An electron with a transverse velocity component that is opposite in direction to that of the electric field gains energy (γ increases), so that its cyclotron frequency decreases and the electron begins falling behind the phase of the oscillating electric field. An electron with a transverse velocity component that is in the same direction as the electric field loses energy (γ decreases), so that its cyclotron frequency increases and the electron begins to overtake the phase of the electric field. After many orbits, electrons that were initially distributed uniformly with respect to the phase of the electric field become tightly bunched in phase [9]. This is illustrated in Fig. 2.2 for four test electrons. Net energy is extracted from the bunched electrons if the frequency of the oscillating electric field is somewhat greater than the cyclotron frequency, so that the electron bunches are situated in the decelerating phase of the electric field.

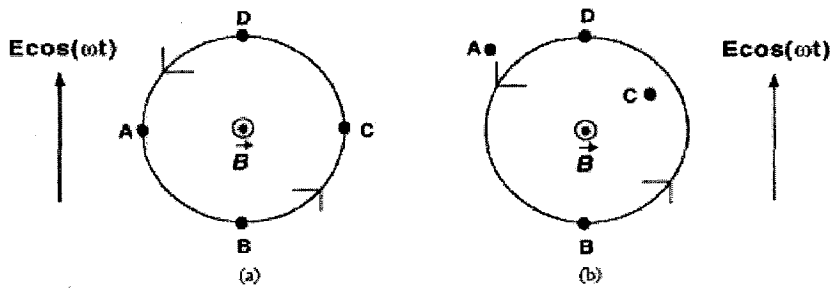

Figure 2.2: (a) Four test electrons rotating in the presence of an applied magnetic field at the beginning of the cyclotron resonance maser interaction. (b) Electron positions after several orbits in the presence of an electric field that oscillates with a frequency that is equal to the electron cyclotron frequency [9].

Gyrotron oscillators (Fig. 2.1) are devices which usually utilize only weakly relativistic electron beams with high transverse momentum. The wave vector of the

radiation in the cavity is almost transverse to the direction of the external magnetic field ($k_\perp >> k_z$, and the Doppler shift is small) resulting, according to (2.1) and (2.2), in radiation near the electron cyclotron frequency or one of its harmonics [15]:

$$\omega \cong s\Omega_c, s = 1, 2, ... \tag{2.3}$$

In cylindrical cavity gyrotrons with radius R_0 the operating mode is close to cutoff ($v_{ph} = \omega/k_z >> c$) and to keep the electron bunches in the retarding phase the frequency mismatch $\omega - s\Omega_c$ is small but positive. The Doppler term $k_z v_z$ is of the order of the gain width and is small compared to the radiation frequency. Cyclotron harmonic operation reduces the required magnetic field for a given frequency by the factor s. The dispersion diagrams of fundamental and harmonic gyrotrons are illustrated in Figs. 2.3a and 2.3b, respectively. However, measured efficiencies of gyrotrons operating at higher harmonics (s=2&3) are lower than those operating at the fundamental frequency.

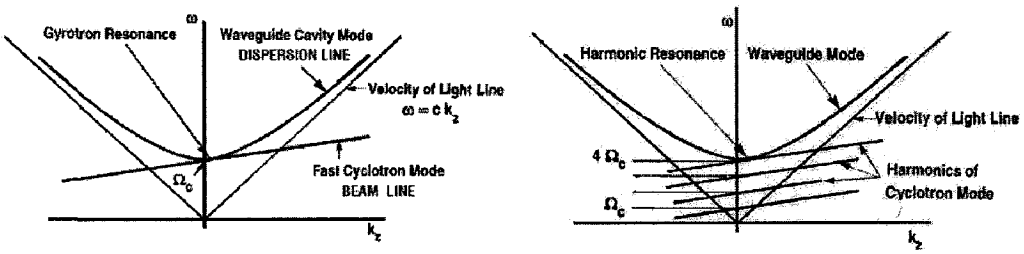

(a) Fundamental Resonance (b) Harmonic Frequency

Figure 2.3: Dispersion diagram of gyrotron oscillator [1].

Many other types of microwave sources are also based on the ECM instability, such as the gyro–klystron, gyro–twystron, gyro–travelling wave amplifier (gyro–TWT) or the gyro–backward wave oscillator (gyro–BWO).

2.2 Theory of Gyrotrons

This section presents the practical considerations for gyrotron design, keeping in mind the design constraints. In addition, the theory behind the starting current calculations and beam–wave interaction has been discussed.

2.2.1 Design Feasibility – Mode Selection

The design of a particular gyrotron always involves tradeoffs among a number of mutually incompatible design goals and constraints. The general design constraints for high power gyrotrons are shown in Table 2.1. The values of all these constraints are calculated for all the candidate modes of the particular gyrotron. These are analyzed comparatively and only that mode is selected as the operating mode for which all the constraints fall within limits.

Table 2.1: Gyrotron Design Constraints.

Peak Ohmic wall Loading (ρ_{wall})	< 2.0 kW/cm^2
Voltage Depression ($\Delta V/V$)	< 0.1
Ratio of beam current to limiting current (I_b/I_L)	< 0.5
Magnetic Compression ($b_{comp} = B_{cav}/B_{gun}$)	< 50
Electric Field at the Emitter(E_e)	< 7 kV/mm
Emitter mean radius (R_e)	< 50 mm
Cathode Current Density (j_e)	< 4 A/cm^2
Fresnel Parameter (C_F)	≈ 1.0

The first four constraints given in Table 2.1 are related to electron beam physics whereas the emitter radius and the corresponding current density are technological constraints. The major physical constraints that limit the operating parameters of a gyrotron are wall loading, voltage depression and limiting current. The voltage

depression and limiting current are problems related to the beam quality which has a direct influence on the resonance condition and interaction mechanism.

Wall Loading

The major constraint for CW gyrotrons is the peak ohmic wall loading ρ_{wall}. This is calculated by integrating the RF power flow into the cavity walls, dividing by the surface area. The ohmic losses are given by [4, 16]:

$$\left(\frac{dP}{dA}\right)_{max} \approx \sqrt{\frac{8}{\pi}} \sqrt{\frac{1}{\pi Z_0 \sigma}} \frac{PQ}{L\lambda^{1.5}} \frac{1}{x_{mp}^2 - m^2} \tag{2.4}$$

where L is the length parameter of the effective Gaussian field profile and $Z_0 \approx 377\,\Omega$ is the impedance of free space. For $\sigma = 3 \times 10^5\ (\Omega\ cm)^{-1}$ (corresponding to ideal hot copper) and $\lambda = 0.714$ cm, this gives

$$\left(\frac{dP}{dA}\right)_{max} \approx 0.0393\ kW/cm^2\ \frac{P}{200\ kW} \frac{Q\lambda}{L} \frac{1}{x_{mp}^2 - m^2}. \tag{2.5}$$

Voltage Depression

It is the reduction of the potential within the beam tube with respect to the cavity wall due to the beam space charge. The voltage depression for a hollow beam of radius R_b is given by [4, 16]:

$$\Delta U_b \approx 60\Omega \cdot \frac{I_b}{\beta_z} \cdot \ln\left(\frac{R_0}{R_b}\right) \tag{2.6}$$

where R_b is the beam radius, I_b is the beam current, and β_z is the axial velocity ratio in the units of c. It is assumed that the guiding center radius is much larger than the beam thickness.

Limiting Current

The limiting current is the current for which the voltage depression becomes so large

that the beam cannot propagate. It should be at least twice as large as the operating current. It is given by [4, 16] as:

$$\frac{I_L}{8500|_A} \approx \frac{I^*}{\ln\left(\frac{R_0}{R_b}\right)} \tag{2.7}$$

$$I^* = \gamma_0 \left[1 - \left(1 - \beta_{z0}^2\right)^{1/3}\right]^{3/2} \tag{2.8}$$

with $\beta_z = [1 - \beta_\perp^2 - 1/\gamma^2]^{1/2}$. Here γ_0 and β_{z0} represent the values in the absence of voltage depression.

Fresnel Parameter

Russian researchers introduced a parameter called the *Fresnel parameter* (C_F) which can influence how a particular mode oscillates [4]. It is defined as

$$C_F = \frac{L^2}{8R_0\lambda\sqrt{1 - \left(\frac{m}{x_{mp}}\right)^2}}. \tag{2.9}$$

where L is the effective length of the interaction region. It describes the effective diffraction of a wave at the taper transitions in a resonator. For TE modes near cut–off, $(2\pi/\lambda) \simeq (x_{mp}/R_0)$ which simplifies the expression for the Fresnel parameter as:

$$C_F \cong \frac{\pi}{4} \cdot \frac{\left(\frac{L}{\lambda}\right)^2}{\sqrt{x_{mp}^2 - m^2}}. \tag{2.10}$$

Though this modified expression (2.10) is considered as the original definition for the Fresnel parameter but the relevance of the cavity radius R_0 in C_F as given in (2.9) is much more important. According to Gaponov [17], cavities with $R_0 \geq L$, the Fresnel parameter is rather small $C_F < 1$. This gives an unfixed longitudinal and transverse structure of the RF field. Therefore, it may be interpreted that in the case of operation with higher modes when $R_0 \geq L$, the fixation of the longitudinal and transverse structure of the RF field is difficult [4]. So it is probable that a value of $C_F > 0.5$ is desirable, but $C_F \geq 1$ is not necessary.

2.2.2 Starting Currents

A gyrotron will not oscillate if the current is below a threshold value I_{start}, which depends on the beam properties, magnetic field, resonator geometry, etc. The starting currents provide an estimate of the segregation of the different modes in the frequency domain, also taking into account their coupling to the electron beam. The purpose is to estimate how well the mode of interest is separated from possible competing modes that also couple well to the electron beam. The starting current by definition [4], is the minimum current for which $dP_{out}/dt > 0$ in the limit $P_{out} \longrightarrow 0$:

$$I_{start} = \left(U \frac{d\eta}{dP}\bigg|_{P=0} \right)^{-1} \tag{2.11}$$

Stable operation is possible only when $I > I_{start}$, and $dP_{out}/dI_b > 0$, otherwise oscillation will not start at the operating point under consideration. To initially compute the starting currents of main mode and its competitors for preliminary assessment, a Gaussian field profile is employed.

The starting current can be calculated in a linearized single-mode theory. This has been given in detail in [4].

$$\begin{aligned} \frac{-1}{I_{start}} = & \left(\frac{QZ_0 e}{8\gamma_0 m_e c^2} \right) \left(\frac{\pi}{\lambda} \int_0^L |f_{mp}(z)|^2 \, dz \right)^{-1} \\ & \cdot \left(\frac{k_{mp} C_{mp} G_{mp}}{\beta_{z0}(s-1)!} \right)^2 \left(\frac{c k_{mp} \gamma_0 \beta_{t0}}{2\Omega_0} \right)^{2(s-1)} \\ & \cdot \left(s + \frac{1}{2} \frac{\omega \beta_{t0}^2}{v_{z0}} \frac{\partial}{\partial \Delta_s} \right) \cdot \left| \int_0^L \hat{f}(z) e^{i\Delta_s z} dz \right|^2 . \end{aligned} \tag{2.12}$$

where

$$\Delta_s(z) = \frac{\omega}{v_{z0}}\left(1 - \frac{s\Omega_0(z)}{\omega\gamma_0}\right)$$

$$Z_0 = \sqrt{\mu_0/\epsilon_0} \simeq 377\Omega$$

$$k_{mp} = \frac{x_{mp}}{R(z)}$$

$$G_{mp} = J_{m-s}(k_{mp}R_e) \quad \text{for co} - \text{rotating modes}$$

$$= (-1)^s J_{m+s}(k_{mp}R_e) \text{ for counter rotating modes}$$

The important point for this study is that the starting current is inversely proportional to the beam–field coupling constant:

$$\frac{J^2_{m\pm s}\left(\frac{x_{mn}R_e}{R_o}\right)}{\pi(x^2_{mn} - m^2)J^2_m(x_{mn})} \tag{2.13}$$

If this is too small for a given mode, the starting current will be large and the mode is unlikely to oscillate [18]. If starting current is too high, then rise times of field and current can be comparable and field cannot react fast enough to a change in the current. This becomes a problem in the pulsed mode.

2.2.3 Beam–wave Interaction

The gyrotron cavity is where the electron beam transfers energy to the transverse electric field mode. This is popularly known as beam–wave interaction that involves the precarious design of cold cavity structure (interaction circuit) and the study of RF–behavior.

Interaction Structure

The design of resonators for gyrotron oscillators requires the knowledge of the RF field profile, resonator eigenfrequencies, and quality factor Q. With a good design, the microwave radiation can be extracted at high efficiency levels. In conventional gyrotrons, the cavity is a standard three section structure with an input taper and a uniform mid–section followed by an output uptaper as shown in Fig. 2.4. The input taper is a cut–off section which prevents the back propagation of RF power to the gun. Parabolic smoothing of the input and output tapers is carried out to reduce unwanted mode conversion at sharp transitions. The beam–wave interaction takes place in the uniform mid–section where the RF–fields reach peak values. The uptaper with nonlinear contour connects the cavity with output waveguide and launcher of the quasi–optical output coupler.

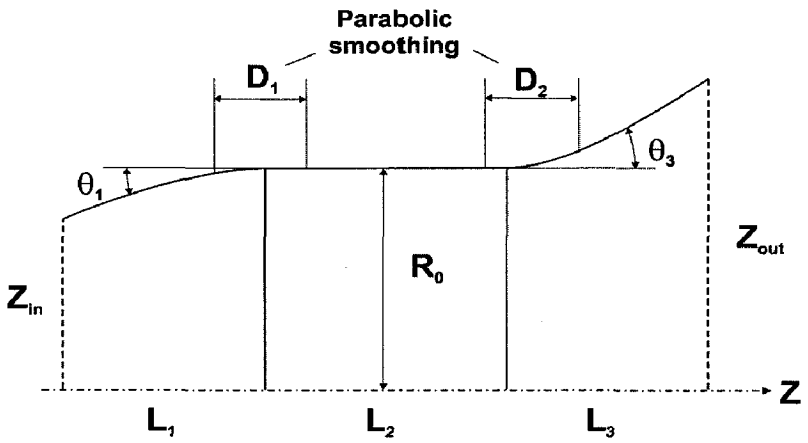

Figure 2.4: Resonator geometry [4].

Reflections at tapers lead to resonant behavior of the apparatus; Q is a measure of the efficiency with which a wave is transmitted out of the resonator. The resonance frequency ω and the quality factor Q are determined by the boundary conditions at the resonator output section [4]. The basic procedure to determine the eigenmodes in an open–ended cavity is to solve the wave equation in the cavity geometry by applying radiation boundary conditions for minimum reflections to obtain resonant

frequencies of the eigenmodes.

The physical electric and magnetic fields are obtained by taking the real part of the complex phasor multiplied by $e^{i\omega t}$ as given in [19], i.e.

$$\vec{E}(\vec{r},t) = Re\left[\vec{E}(\vec{r})e^{i\omega t}\right] \tag{2.14}$$

The complex phasor for a TE_{mp} mode is given explicitly by

$$\begin{aligned} E_z &\simeq 0 \\ E_r &= \pm im\frac{\Psi_{mp}}{r}f(z) \\ E_\theta &= \frac{\partial\Psi_{mp}}{\partial r}f(z) \end{aligned} \tag{2.15}$$

with

$$\Psi_{mp} = C_{mp}J_{mp}\left(x_{mp}\frac{r}{R(z)}\right)e^{im\theta}$$

From $-\partial\vec{B}/\partial t = \vec{\nabla}\times\vec{E}$, we obtain

$$\begin{aligned} i\omega\mu H_z &= \left(\frac{x_{mp}}{R(z)}\right)^2 f(z)\Psi_{mp} \\ i\omega\mu H_r &= \frac{\partial E_\theta}{\partial z} \\ i\omega\mu H_\theta &= -\frac{\partial E_r}{\partial z} \end{aligned} \tag{2.16}$$

$$C_{mp} = \frac{1}{\sqrt{\pi(x_{mp}^2 - m^2)}}\frac{1}{J_m(x_{mp})}$$

is a normalization constant introduced such that

$$2\pi\int_0^R r|E|^2dr = |f(z)|^2$$

As a first approximation, *f(z)* which describes the longitudinal variation of the mode, is obtained by solving an approximate equation due to Vlasov [20]:

$$\frac{d^2f}{dz^2} + k^2(z)f = 0 \tag{2.17}$$

Here f describes the longitudinal variation of a TE or TM mode, and k is the mode propagation factor. The eigenfunctions of an open resonator which are of interest in gyrotron design correspond to solutions of boundary conditions, which have the form of an outgoing wave at the resonator output. If the resonator dimensions are such that the working mode is cut–off at the input section and propagating in the output section, the appropriate radiation boundary conditions at the resonator input and output boundaries are:

$$\frac{df}{dz} - ikf = 0 \quad at\ z = z_{in} \tag{2.18}$$

$$\frac{df}{dz} + ikf = 0 \quad at\ z = z_{out} \tag{2.19}$$

z_{in} and z_{out} are the input and output radius as shown in Fig. 2.4 which depicts a typical gyrotron resonator. Also $k^2(z) = \omega^2/c^2 - x_{mp}^2/R(z)^2, where\ x_{mp}$ is the p'th root of $J'_m(x)$ and R(z) defines the cavity profile. We take Re[k]>0 if Re[k^2]> 0 and Im[k] < 0 when Re[k^2]< 0. It is assumed that $|Re[k^2]| \gg |Im[k^2]|$ and that $|dk/dz| \ll k^2$. When Q is finite, the source free resonator fields decay exponentially in time, as expected. This corresponds physically to the fact that the electromagnetic fields propagate out of the resonator. It is convenient to normalize the *f(z)* such that the output power at z_{out} is fixed. From Poynting's theorem we have

$$P_{out} = \pi \int_0^R rdr\,(Re\ E \times H^*)_z \Big|_{z=z_{out}} \tag{2.20}$$

Applying the boundary conditions we obtain,

$$P_{out} = Re\frac{1}{2\mu\omega}k^*\,|f(z_{out})|^2 \tag{2.21}$$

In single mode approximation, Vlasov equation reduces to

$$\frac{d^2V_{mq}}{dz^2} + \left(\frac{\omega^2}{c^2} - k_{mq}^2\right)V_{mq} \simeq +i\omega J_{mq}. \tag{2.22}$$

CENTRAL LIBRARY
G 20077
ACC No.....
Date.....
I. T. ROORKEE

where J_{mq} is the source term given in [4].

The solution of the above simplified equation (2.22) is best carried out with the Numerov algorithm when $J_{mq} = 0$. The formalism given here is valid when cavity profile $R(z)$ is continuous and differentiable. If $R(z)$ has discontinuities, then the equations must be solved piecewise and the fields and their derivatives have to be matched at the discontinuities of $R(z)$.

For numerical calculations, the boundary condition at z_{in} is used to determine the starting value of $\partial V/\partial z$. The boundary condition at z_{out} is reformulated in the form

$$|R| = \left| \frac{\frac{dV}{dz} + ik_z V}{\frac{dV}{dz} - ik_z V} \right| = \text{minimum} \tag{2.23}$$

One could also specify a non-zero reflection coefficient R_{load} such that the condition $|R - R_{\text{load}}| = minimum$, is imposed.

It is convenient to work with a normalized field profile. This will be done by defining

$$V_{mp}(z) = V_{max} \hat{f}_{mp}(z) \tag{2.24}$$

Here, $\hat{f}_{mp}(z)$ is the field profile normalized to a maximum absolute value 1. In the cold cavity approximation, V_{max} and the output power are related by:

$$QP_{\text{out}} = \omega W = \left(\frac{\omega \epsilon_0}{2}\right) V_{\text{max}}^2 \int_{z_{\text{in}}}^{z_{\text{out}}} \left| \hat{f}_{mp}(z) \right|^2 dz. \tag{2.25}$$

RF–Behavior

The equation of motion for a single electron traversing the resonator in the given electric and magnetic fields must be solved numerically to compute the efficiency, output power and energy loss or gain. The efficiency is then computed by averaging over an ensemble of electrons uniformly distributed in their initial gyration phase angle. The fact that the electrons gyrate rapidly around the guiding center facilitates the numerical solution of the equation of motion. The approximation of

neglecting the RF magnetic fields and guiding center drift, and taking advantage of the fact that maximum energy transfer takes place when the electron gyration is approximately synchronous with a rotating field component, to an approximate one dimensional equation is known as the adiabatic approximation.

In cold cavity calculations, the adiabatic approximation to equation of electron motion is derived and this equation of motion is solved in the fixed field approximation to compute the efficiency. In self–consistent calculations, the equation of motion is solved simultaneously with the field equations, taking into account the effect of beam on the cavity field profile and quality factor, as well as frequency pulling.

The equations describing gyrotron operation at arbitrary harmonics have been explained long back as in [21,22]. A derivation for the conventions used here is given, for example, in [23,24]. Define

$$\vec{u} = \gamma\vec{v}/c \tag{2.26}$$

and

$$P = iu_{\perp}e^{-i(\Lambda+\theta_e)} = u_{\perp 0}\tilde{P} \tag{2.27}$$

where Λ is the slowly varying part of the gyrophase. The equation of motion for the electrons in the field of a TE_{mp} mode can be reduced to

$$u_z \approx constant \tag{2.28}$$

$$\begin{aligned} \frac{d\tilde{P}}{dz} &+ i\frac{\omega}{v_{z0}}\frac{1}{s}\left(\frac{\gamma}{\gamma_0} - 1 + \delta\right)\tilde{P} \\ &= i\frac{\omega}{v_{z0}}\frac{\gamma}{\gamma_0}F_{mp}\hat{f}_{mp}(z)\left(\frac{ck_{mp}u_{\perp 0}\tilde{P}^*}{2\Omega_0}\right)^{s-1} \end{aligned} \tag{2.29}$$

Here $\hat{f}(z)$ is the normalized field profile, δ is detuning parameter

$$\delta = 1 - \frac{s\Omega_0}{\gamma_0 \omega} \tag{2.30}$$

and

$$F_{mp} = \frac{eV_{max}}{2mc^2} \frac{C_{mp}G_{mp}}{u_{\perp 0}} \frac{ck_{mp}}{\omega} \frac{1}{(s-1)!} \tag{2.31}$$

is related to the similar quantity used by [12,25] as

$$F_G = \left(\frac{s\beta_\perp^2}{2}\right)^{s-2} F_{mp} \tag{2.32}$$

Also

$$C_{mp}G_{mp} = \pm \frac{J_{m\pm s}(k_{mp}R_e)}{J_m(x_{mp})\sqrt{\pi(x_{mp}^2 - m^2)}} \tag{2.33}$$

The output power in the TE_{mp} mode is given by the Poynting vector. One can show that [23]:

$$P_{out} = V_{max}^2 Re\left(\frac{1}{2i\mu_0\omega} \hat{f}_{mp} \frac{d\hat{f}_{mp}^*}{dz}\right) \tag{2.34}$$

evaluated at the resonator output. Also note that

$$\frac{ck_{mp}u_{\perp 0}}{2\Omega_0} \simeq \frac{s\beta_{\perp 0}}{2}$$

In a self–consistent formulation, the field profile satisfies

$$\frac{d^2F_{mp}\hat{f}}{dz^2} + \left(\frac{\omega^2}{c^2} - k_{mp}^2(z)\right) F_{mp}\hat{f} = -\tilde{I}\left(\frac{-ick_{mp}u_{\perp 0}}{\Omega_0}\right)^{s-1} \langle \tilde{P}^s \rangle \tag{2.35}$$

Here

$$\tilde{I} = \frac{eZ_0 I_b}{2mc^2} \left(\frac{C_{mq}k_{mp}G_{mp}}{(s-1)!}\right)^2 \cdot \frac{1}{u_{z0}}$$

where I_b is the beam current, $Z_0 = \sqrt{\frac{\mu_0}{\epsilon_0}}$ and $k_{mp}(z) = \frac{x_{mp}}{R(z)}$, with radiation boundary conditions at the output.

2.3 Components of Gyrotron

Single–mode mm–wave gyrotrons capable of producing high average power ($0.5 - 1$ MW per tube) in long–pulse or CW operation, are currently under development in several scientific and industrial laboratories. A modern gyrotron consists of the following main units.

2.3.1 MIG and Magnet System

Gyrotrons need a high power, hollow, electron beam with sufficient orbital energy and small velocity spread. The development of powerful magnetron injection guns (MIGs) for gyrotrons has played a major role in making these devices powerful coherent radiation sources. The MIGs produce annular electron beams in which electrons execute small cyclotron orbits at a frequency required for cyclotron resonance interaction in a gyrotron. The schematic outline of a triode–type magnetron injection gun is shown in Fig. 2.5.

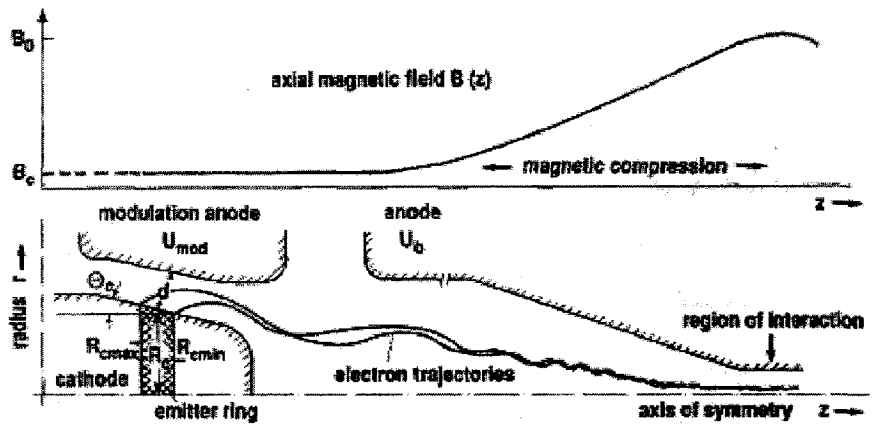

Figure 2.5: Schematic outline of a triode–ype magnetron injection gun (MIG) with two anodes and plot of a typical magnetic field profile [26].

For frequencies above 30 GHz where magnetic field strengths in excess of 1 T are required for operation at the fundamental cyclotron resonance in a gyrotron, su-

perconducting magnet coils are generally employed. The magnetic field strength in Tesla for a given frequency is approximately equal to $f\ (GHz).\gamma/28$, where f is the operating frequency in GHz and γ is the relativistic factor. Most magnets usually consist of one or two main cavity magnet coils and a gun coil to adjust the magnetic field strength in the vicinity of the cathode. Magnet coils employed to shape the magnetic field profile in the collector are also usually room–temperature coils. The superconducting coils are usually made from Nb_3Ti wire and cooled using liquid helium.

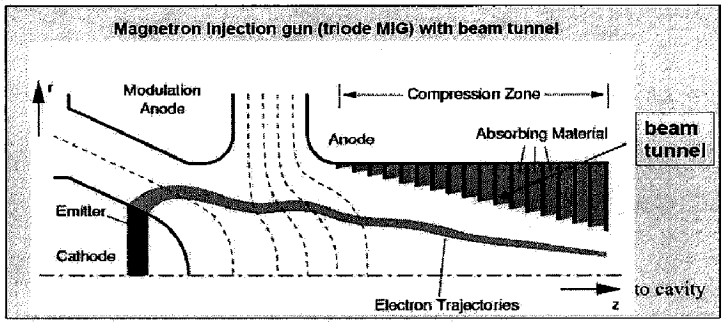

Figure 2.6: Schematic of MIG with the Electron Beam Tunnel [4].

The region starting from the MIG and ending at the entrance of the interaction cavity is called the beam tunnel (Fig. 2.6). In this compression region the wall and electron beam radii are reduced from starting till the end. The beam tunnel usually has a sophisticated alternating metal–damping ceramics ring structure. This ring structure has specially shaped rings of lossy ceramics to suppress spurious oscillations and beam instabilities.

Trade–off and initial design expressions for a Magnetron Injection Gun are described below [4]. The most important parameters for the gun design are given here. The initial design establishes the main gun parameters such as cathode radius (average), cathode–anode spacing, emitter current density, electric field at the cathode, and the cathode slant angle to the required beam properties. After that the simulation

codes are used for a final optimization of the shape of the electrodes.

- Electron energy U_b and relativistic mass factor:

$$\gamma_0 = 1 + \frac{U_b}{511\,\mathrm{kV}} = \frac{1}{\sqrt{1-\beta_{\perp 0}^2-\beta_{z0}^2}} \tag{2.36}$$

- Beam power $U_0 I_b$, where U_0 is the accelerating voltage and I_b is the total beam current.

- Optimum cyclotron frequency:

$$\omega_c = \frac{eB_0}{m_e\gamma_0}. \tag{2.37}$$

- Larmor radius at interaction:

$$r_{L0} = \frac{v_{\perp 0}}{\omega_c} = 1.705\,\mathrm{mm} \times \frac{\gamma_0\beta_{\perp 0}}{B(\mathrm{T})} \tag{2.38}$$

- Velocity ratio:

$$\alpha = \frac{v_{\perp 0}}{v_{z0}} \tag{2.39}$$

- The radial thickness of the beam at interaction should not exceed $\lambda/8 + 2r_{L0}$.

The other parameters should be chosen to provide the above beam parameters with minimal velocity spread. These include:

- Compression ratio:

$$b = \frac{B_0}{B_c} \tag{2.40}$$

- Emitter Radius: From Busch's theorem, the cathode radius is related to the beam radius (in paraxial approximation) by

$$R_c = \sqrt{b}R_e \tag{2.41}$$

and the emitter radius thickness can be estimated from

$$\Delta R_c = \sqrt{b}\Delta R_e. \tag{2.42}$$

- Emitter Length: Simple geometry determines the emitter length l_s from total current

$$I_b = (2\pi R_c l_s) J_c, \tag{2.43}$$

where ϕ_c is the cathode slant angle and J_c is the cathode current density, note that (also)

$$\Delta R_c = l_s \sin \phi_c. \tag{2.44}$$

- Cathode electric field: A first estimate of the required cathode electric field E_c can be obtained from

$$\gamma_0 v_{\perp 0} = \sqrt{b}\gamma_c v_{\perp c} = \frac{\sqrt{b} E_c \cos \phi_c}{B_c}, \tag{2.45}$$

and this requires

$$E_c \cos \phi_c = \frac{B_0 \gamma_0 v_{\perp 0}}{b^{3/2}}. \tag{2.46}$$

- Cathode–anode spacing: The cathode–anode spacing (d) is given by

$$d = R_c \frac{r_{L0} D_F \mu}{\cos \phi_c}, \tag{2.47}$$

where D_F is the cathode–anode spacing factor (select $D_F \geq 2$) and μ is Tsimring cylindricity parameter ($= 1/\sqrt{(r_{g0}/r_{L0})^2 - 1}$ and r_{g0} is the guiding center radius at the RF interaction region).

2.3.2 Interaction Cavity

The interaction cavity for most gyro–oscillators consists of a simple cylinder with a down taper at the cavity entrance and an up taper at the cavity exit (Fig. 2.7). These devices operate most effectively near the cut–off frequency of the desired TE mode in the cavity. This enables the mild tapers at the entrance and exit of the cavity to provide enough reflection to maintain a standing wave in the cavity. The frequency of the resulting $TE_{m,p,q}$ resonance is set to correspond to the desired operating frequency, which in turn must satisfy the cyclotron resonance condition in

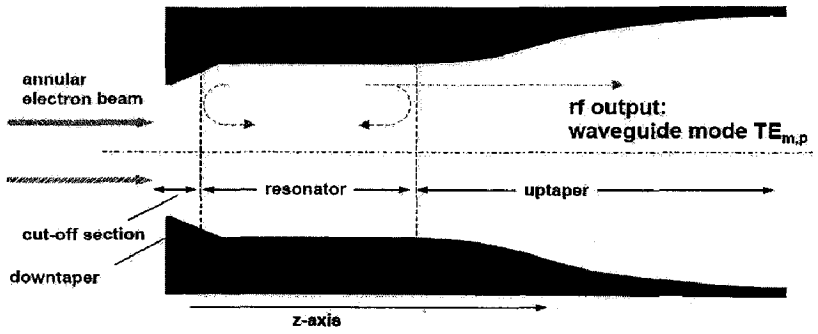

Figure 2.7: Schematic of Interaction Cavity.

(2.1). The beam–wave interaction has already been discussed in previous section.

One of the major advantages of gyrotrons is that the interaction is relatively insensitive to the beam quality, especially in oscillators [27]. At the same time one of the most important problems in the design of high-power high-frequency gyro–scillators is ensuring operation in the desired mode. The design trade–offs that determine the choice of cavity modes are:

- ohmic wall losses in the cavity ($P_{max} < 2kW/cm^{-2}$),
- beam voltage depression($R_e/R_0 \geq 0.5$), where R_e is the electron beam radius,
- selection and mode competition (single–mode operation),
- efficiency considerations ($\approx 35\%$),
- high power requirements (1 MW in CW operation).

All these requirements are met by only rotating high order volume modes (e.g. $TE_{28,8}$ at 140 GHz). The coupling of the desired working mode with beam electrons is strongest if the nominal beam radius in the resonator coincides with the inner electric field maximum (approximately the caustic radius of the mode). The use of dispersion strengthened copper (Cu: Al_2O_3) as cavity material and advanced cooling techniques significantly improve the thermo-mechanical features of the cavity.

2.3.3 Non–linear Taper (NLT)

Tapered transmission lines (tapers) are required to transform the output of a standard waveguide to oversized waveguide components. The taper should be designed in such a way that the characteristic impedances at both the ends are matched. Two basic types of cross–section tapers are straight taper and variable (non–linear) taper. In the straight taper, the taper angle is fixed throughout the length and abrupt discontinuities occur at both the ends, while in variable taper the taper angle is smoothly varied along the length of the taper. The advantage of a non–linear taper is that the conversion of power to unwanted (spurious) modes is very less compared to straight taper [4]. Different types of basic waveguide tapers are shown in Fig. 2.8.

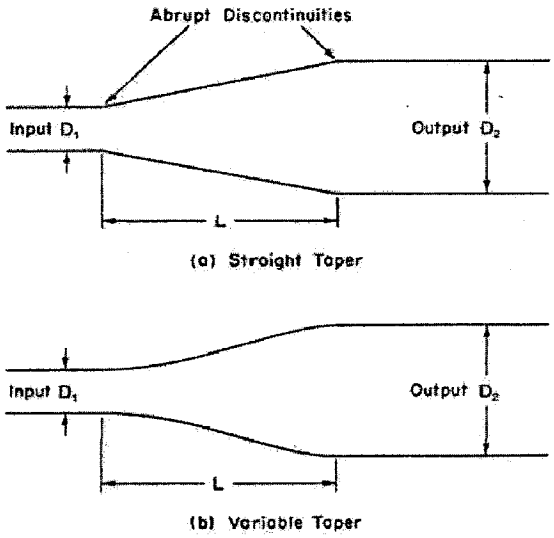

Figure 2.8: Different types of Tapers [4].

In gyrotrons, the non–linear taper is used to connect the interaction region with the output waveguide system. The main challenge in the design of a non–linear taper for gyrotron is that it requires very high transmission (above 99%) with very less spurious mode generation. Due to high output power, even 1% of reflections cause severe damage to the entire system. For this reason, although it is a simple component, it has to be designed very carefully.

The main difficulties in the design of gyrotron output tapers in comparison with highly oversized waveguide tapers are as follows:

- Input reflections as well as forward and backward scattered waves must be considered at the taper input, as the working mode is very close to cut off.
- The ratio of the collector to the cavity output radii is very large for conventional gyrotrons with axial output coupling. This can lead to a strong excitation of many parasitic modes.
- Mode coupling occurs as higher order working modes tend to couple to higher and lower undesired neighboring azimuthally symmetric modes. TE_{mn} modes with $n > 0$ couple not only to TE_{mq} modes but also excite TM_{mq} modes.

The presence of a taper in a waveguide introduces unwanted parasitic modes. Gyrotron output tapers should act as a near perfect match at the input port with suppressed spurious modes at the output port with a taper length as short as possible. Conical tapers with constant cone angle introduce a higher degree of parasitic modes which is not preferable. Tapers with gradual change in the cone angle cause considerably less power conversion to spurious modes. Since all the gyrotron output tapers are cylindrically symmetric, their performance does not depend on the sense of the rotation of the mode. The principle methods employed for the analysis and synthesis of gyrotron output tapers are given in detail in [4] and the references therein.

In the present work, a raised–cosine profile has been used for the taper design. A schematic diagram of a raised–cosine taper is shown in Fig.2.9. The synthesis of this taper profile was carried out using the following formulae [28]:

$$\alpha = -1.0 + 2.0\left(\frac{i}{l}\right)^{\gamma} \tag{2.48}$$

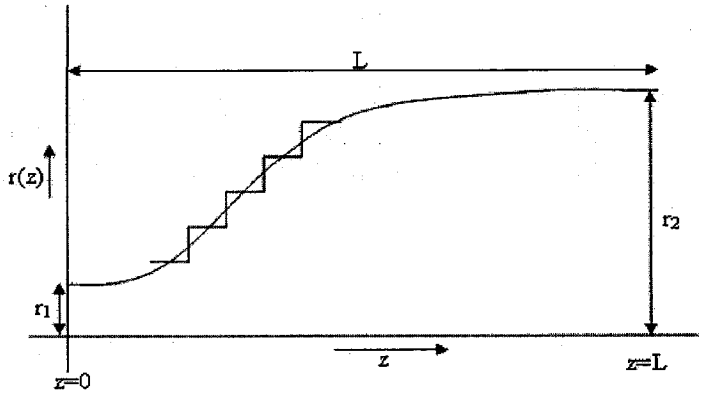

Figure 2.9: The raised–cosine taper profile.

$$r(z) = \frac{r_2 - r_1}{2} \cdot \left(\alpha + \frac{1}{\pi} sin(\pi\alpha)\right) + \frac{r_2 - r_1}{2} \tag{2.49}$$

$$r = r_1 + r(z) \tag{2.50}$$

2.3.4 Quasi–optical (QO) Mode Converter

In the gyrotron, the QO mode converter consists of a waveguide launcher (cut), a quasi–parabolic or quasi–elliptical mirror and one to two toroidal mirrors (Fig. 2.10). The QO mode converter placed between the cavity and the output window is intended to convert the gyrotron cavity modes into a linearly polarized Gaussian beam. This beam profile is formed at the aperture prior to the reflectors.

The following requirements for the QO mode converter should be satisfied:

- Low diffraction losses inside the tube (less than 3%)
- Matching of the output wave beam to the HE_{11} waveguide transmission mode or the fundamental Gaussian beam with efficiencies higher than 97%.

A typical and simple example of the mode converter/launcher is a Vlasov type launcher, which consists of a cylinder whose end opening is cut along a helix [29]. A Vlasov–type converter has a simple structure; however, it suffers high diffraction

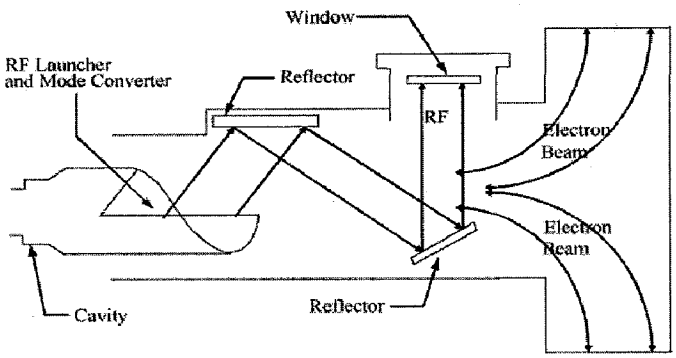

Figure 2.10: Schematic of the Quasi–optical RF output system [30].

loss (15%–20%) at its opening because the beam profile that is formed has an approximately uniform field distribution in the axial and azimuthal directions at the aperture. However, the following methods can be followed to obtain low diffraction losses, resulting in a pencil–like wave beam:

1. Pre–shaping of the wave beam before it is launched. To achieve a sidelobe-free fundamental Gaussian beam as the output mode, the launcher must have space–periodic helical feed waveguide deformations (dimples) such that the incident rotating TE mode is converted to a suitable mode mixture generating the Gaussian beam distribution (Fig. 2.11).

2. In cases where a simple Vlasov launcher is used in connection with a large quasi–parabolic reflector, specific non–quadratic phase–correcting mirrors allow one to generate any desired amplitude and phase distribution of the wave beam.

A brief analysis of the quasi–optical launcher can be done as follows, for details refer [31] and the references therein. Helically propagating TE– and TM– modes in a circular waveguide can be decomposed into a series of plane waves, each propagating at the Brillouin angle θ_B relative to the waveguide axis:

$$\theta_B = \arcsin(x_{mn}/k_0 R_w) \tag{2.51}$$

Figure 2.11: Schematic contour of the Wall Surface of a Dimpled–wall Launcher [31].

- x_{mn} : root of Bessel function
- k_0 : free-space wavenumber
- R_w : radius of the launcher waveguide

The requirement of a zero azimuthal electric field at the waveguide wall defines their relative phases. In the geometric optics limit, a plane wavefront is represented by one ray. Its transverse location is defined by the requirement that the ray direction must coincide with the Poynting vector direction. If the point of interest is located at the waveguide wall the ray has the distance:

$$R_c = \frac{m}{x_{mn}} R_w \tag{2.52}$$

from the waveguide center. Hence if all plane waves are presented by geometric optics rays they form a caustic of radius R_c. In an unperturbed circular symmetric waveguide the density of the rays along the caustic is uniform. The distance that a ray has propagated in the axial direction between two subsequent reflections from the waveguide wall is [32]:

$$L_B = 2R_w \left[1 - \left(\frac{m}{x_{mn}}\right)^2\right]^{1/2} \cot\theta_B \tag{2.53}$$

In the transverse direction a section of angle:

$$\Delta\phi = 2\theta = 2 \arccos\left(\frac{m}{x_{mn}}\right) \tag{2.54}$$

reflects all rays exactly once. Accordingly, reflection points of each of the rays are placed on the waveguide surface in a helical line with the angle of inclination

$$\alpha = \arctan\left(\theta \tan\theta_B / \sin\theta\right) \tag{2.55}$$

and the distance (pitch) that a ray has propagated in the axial direction when it has completed a full turn is [32]:

$$H = 2\pi R_w \cot\alpha = 2\pi R_w \frac{k_z}{k_\perp} \frac{\sqrt{1-(\frac{m}{x_{mn}})^2}}{\arccos(\frac{m}{x_{mn}})} = L_c \tag{2.56}$$

which is the launcher cut length. Hence waveguide sections with the length L_c and the transverse width defined by $\Delta\phi R_w$ reflect each ray once.

The surface deformation points on type–2 surface are calculated on the basis of the studies given by Hirata [30]. The role of the deformation points is to transform the gyrotron cavity mode into a bundle of modes that form a Gaussian intensity profile at the aperture, prior to the reflectors. The deformation points are optimized to maximize the Gaussian content in the beam at the helical cut. The helical converter is described by the following wall perturbation:

$$R(\phi, z) = a + \delta_1 \cos(\Delta\beta_1 z - l_1\phi) + \delta_2 \cos(\Delta\beta_2 z - l_2\phi) \tag{2.57}$$

where

$$\begin{aligned} \Delta\beta_1 &= k_{zm,n} - k_{zm\pm1,n}, l_1 = \pm 1 \\ \Delta\beta_2 &= k_{zm,n} - k_{zm\pm\Delta m,n\pm\Delta n}, l_2 = \pm\Delta m \end{aligned} \tag{2.58}$$

Here, $k_{zm,n}$ is the longitudinal wave number of the $TE_{m,n}$ mode, m and n are the azimuthal and radial indexes, respectively [29]. The required minimal launcher length is

$$L_{min} = \frac{\pi}{|2\beta_{m,n} - \beta_{m+1,n} - \beta_{m-1,n}|} \tag{2.59}$$

2.3.5 RF–Window

As gyrotron is a high power source that operates at a very high frequency, high power levels and good pulse lengths, hence the transmission line system from gyrotron to plasma must be designed to handle these with low losses and low reflection back to the gyrotron. Presently, Electron Cyclotron Heating (ECH) power/pulse length that can be delivered to the plasma is limited by the performance of the window [33].

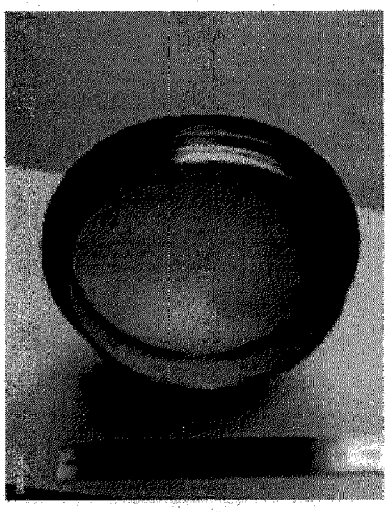

Figure 2.12: Photograph of a diamond CVD disc before installation into a gyrotron with radiation frequency 170 GHz [34].

At present, chemical vapor deposition (CVD) diamond is the only solution for the realization of simple, edge–cooled (water) single–disc 1 MW, CW gyrotron and torus windows. Diamond disks grown by the chemical vapor deposition (CVD) technology (Fig. 2.12) have an exclusive combination of properties [34]:

- a very high heat conductance.
- small microwave losses.
- modest dielectric constant ($\epsilon'_\tau = 5.67 \pm 0.01$).
- low mm–wave attenuation ($tan\delta \approx 2 \times 10^{-5}$).

- mechanical resistance.
- capable of transmitting radiation even with power 2–3 MW.

However, sapphire and SiN windows are also being used in low and moderate power gyrotrons [1] depending upon the output power and operating frequency regime. In the present study, a double–disc face–cooled sapphire RF–window has been employed for output collection.

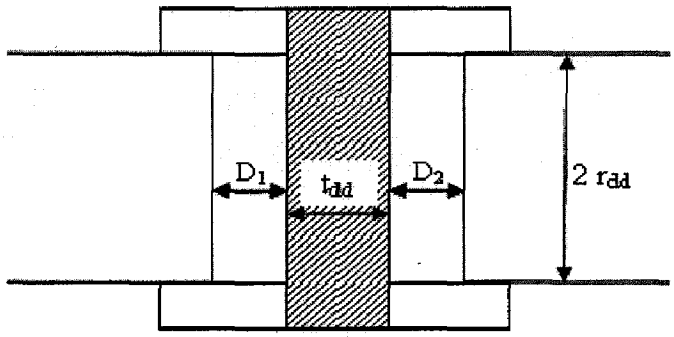

Figure 2.13: Schematic of a double disc RF–window.

The schematic of a double disc window is shown in Fig. 2.13. The value of disc thickness for the TE modes is obtained from the following:

$$D = \frac{\pi}{\sqrt{(\frac{2\pi f\sqrt{\epsilon_r}}{c})^2 - (\frac{\chi_{mn}}{R_{win}})^2}} \tag{2.60}$$

where f is desired resonant frequency, R_{win} specifies radius of the disc, and χ_{mn} is the Bessel root for the $TE_{m,n}$ mode.

2.3.6 Collector

Most of the gyrotron collectors are designed in a way that the electron beam adiabatically follows the diverging magnetic field lines of the gyrotron magnet out to

a diameter where the power density is low enough to safely dissipate the remaining beam power. The efficiency of microwave generation at high frequencies can be improved by floating the collector at a high negative potential thereby retrieving a part of the kinetic energy of the electrons through the electrostatic repulsion between electrons and the collector [35].

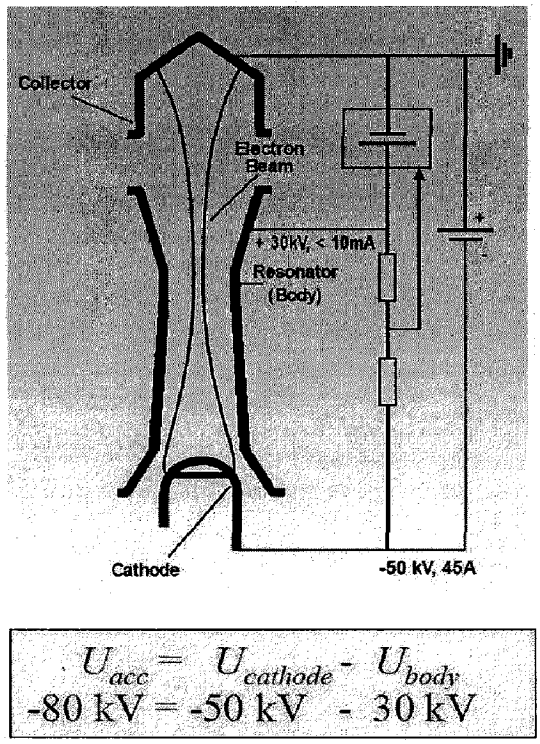

Figure 2.14: Gyrotron with energy recovery system [36].

The electron beam, after the generation of high frequency electromagnetic waves, is decelerated by a decelerating electric field before arriving at the collector, and the decelerated beam energy is recovered by the power supply system, which results in an improvement of gyrotron efficiency (Fig. 2.14). Shaping the collectors and the magnetic field is also necessary to minimize the effect of secondary electrons.

Efficiency may be further increased by spatially splitting the spent electron beam

into several energetic fractions. Then each of the fractions should be collected at an electrode of a properly retarding potential [37]. Since the energy of the spent electron beam is substantially reduced, the total intensity of generated X–rays decreases significantly. It is obvious that all these favorable features bring a large cost reduction of Electron Cyclotron Wave (ECW) systems.

Chapter 3

GDS V.01

A complete Graphical User Interface package "GDS V.01" (Gyrotron Design Suit Ver.01) has been developed for the design of a gyrotron. It is a generalized design package which can be used to design and conceptualize specific gyrotrons. It incorporates the mode selection procedure, starting current calculations, gun synthesis and design of coils, resonator design and RF behavior calculations, launcher design, non–linear taper design and window design. This GUI has been developed in MATLAB R2006a. In this chapter the software has been explained and the design studies are discussed in the next chapter along with the results.

The first screen of the software is as shown in Fig. 3.1. There are two modes of giving input to this software. The first option is to set the values of input parameters in the input files that are provided. While the other option is to fill the forms at run–time to initialize the parameters. Both the methods give the same result. To select between these two options two buttons are provided on the homepage. On clicking on any of these buttons the screen that appears is as shown in Fig. 3.2.

This screen has two panels *Procedure* and *Results*. There are nine different buttons present in the *Procedure* panel for the design of gyrotron. The results are displayed in the *Results* panel. If the *Input File* button is clicked on the homepage then all

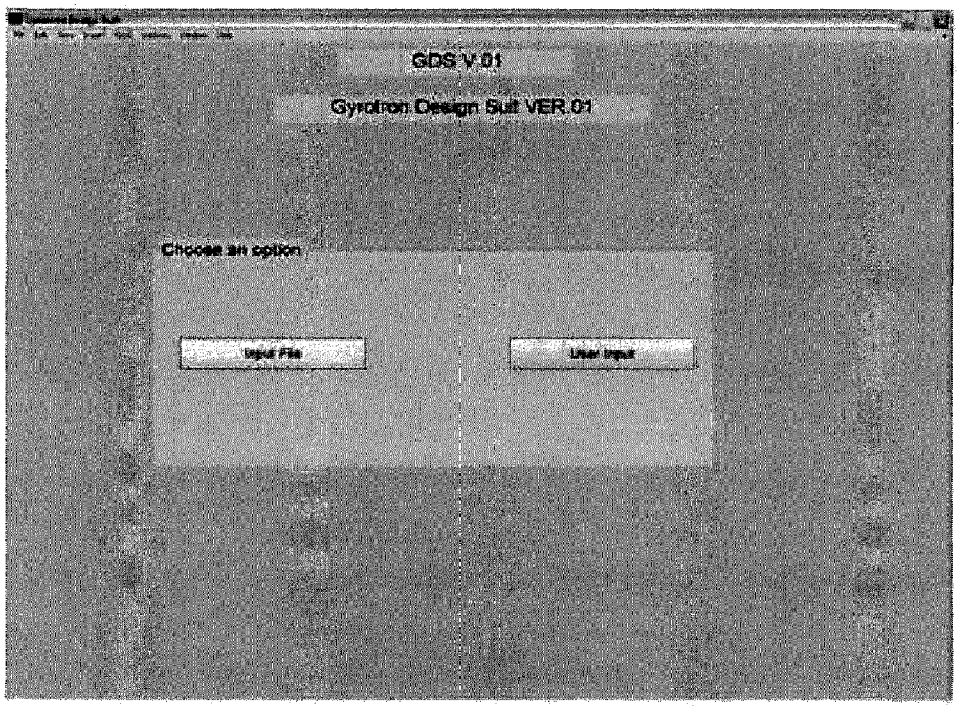

Figure 3.1: GDS Homepage.

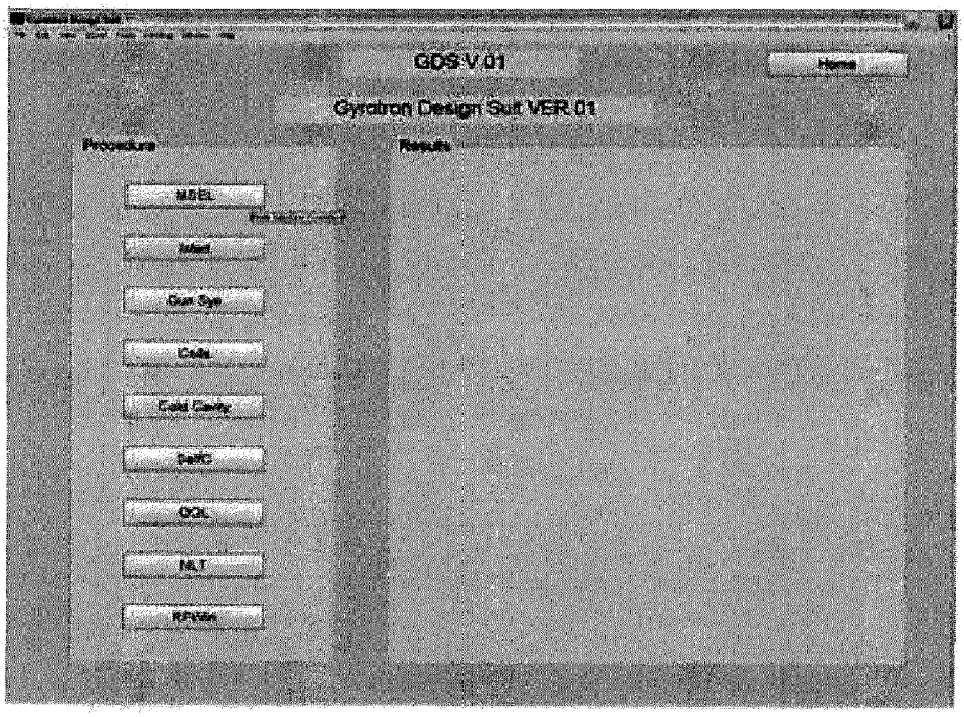

Figure 3.2: Software Modules.

the modules will take parameters from the input files which are present in the folder of this software. On the other hand if the *User Input* button is selected, then forms appear for each module and user has to enter information into these forms.

There is a *Home* button at the top right corner of the page which can be clicked to go back to the homepage and start all over again. Although the buttons are arranged in a manner in which these procedures are generally carried out, but these are independent of each other. This means that any specific procedure can be run by giving its input parameters without the execution of the prior modules. The details of each module are explained in the subsequent sections. The naming of the sections has been done in accordance with the names of the buttons.

3.1 MSEL (Mode Selection)

First step to design any gyrotron is to carry out a mode selection procedure to select the operating mode of the device. So the first procedure in the software is *MSEL* following [4]. In this procedure all the modes between a range of eigenvalues are inspected by calculating all the design constraints for them. These should satisfy the general design considerations. Only the most feasible mode is selected as the operating mode. The design constraints and theory of mode selection have already been covered in chapter 2.

The two snapshots are given in Fig. 3.3 and 3.4 when the two input modes are chosen respectively. As can be seen in Fig. 3.4, when the user input mode is selected, a form appears on the screen where some values need to be entered. On clicking on the *Calculate* button the results appear in the *Results* panel. While the results directly appear in the *Results* panel on clicking the *MSEL* button in the input file mode. The results for the specific gyrotron designed in this work are given in section 4.1.

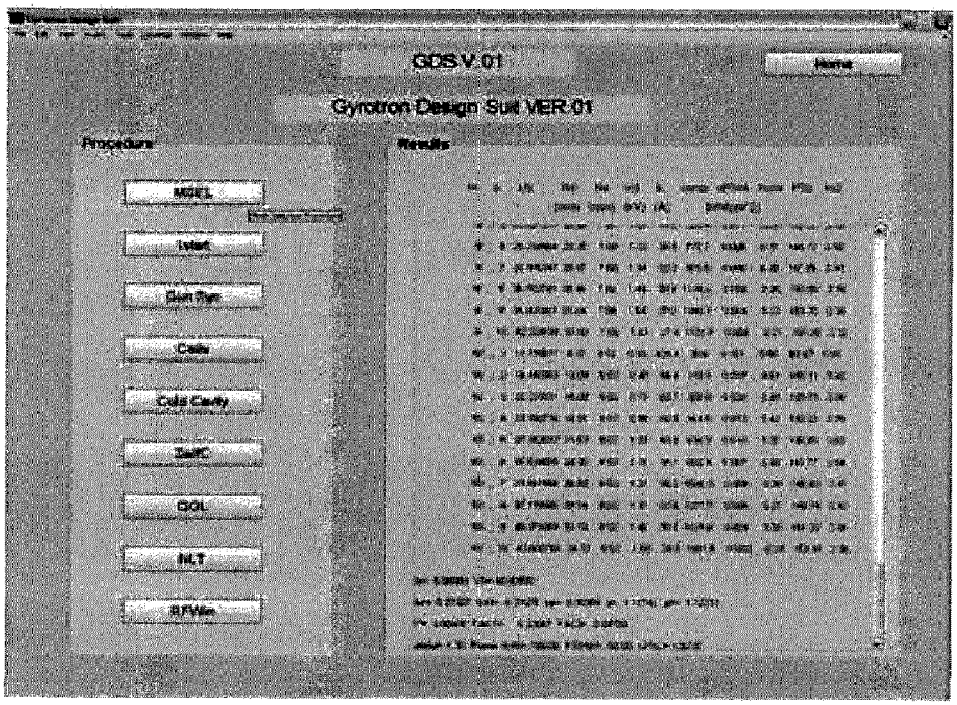

Figure 3.3: MSEL with Input File.

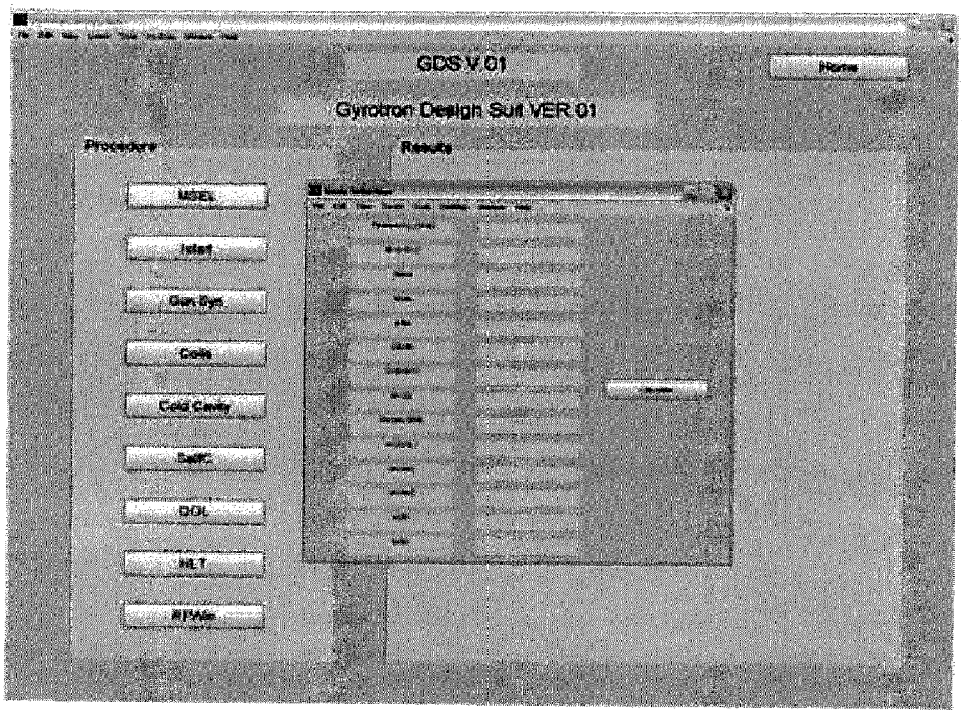

Figure 3.4: MSEL with User Input.

3.2 Istart (Starting Current Calculations)

Once the operating mode is finalized the next step is to do starting current calculations and analyze the mode competition problems. In this procedure the starting current is calculated with respect to the magnetic field for the candidate mode as well as the competing modes on the basis of [4]. On clicking the *Istart* button the starting current values with respect to the magnetic field for the different modes are displayed in the *Results* panel. Also the plot of these values is generated as shown in Fig. 3.5.

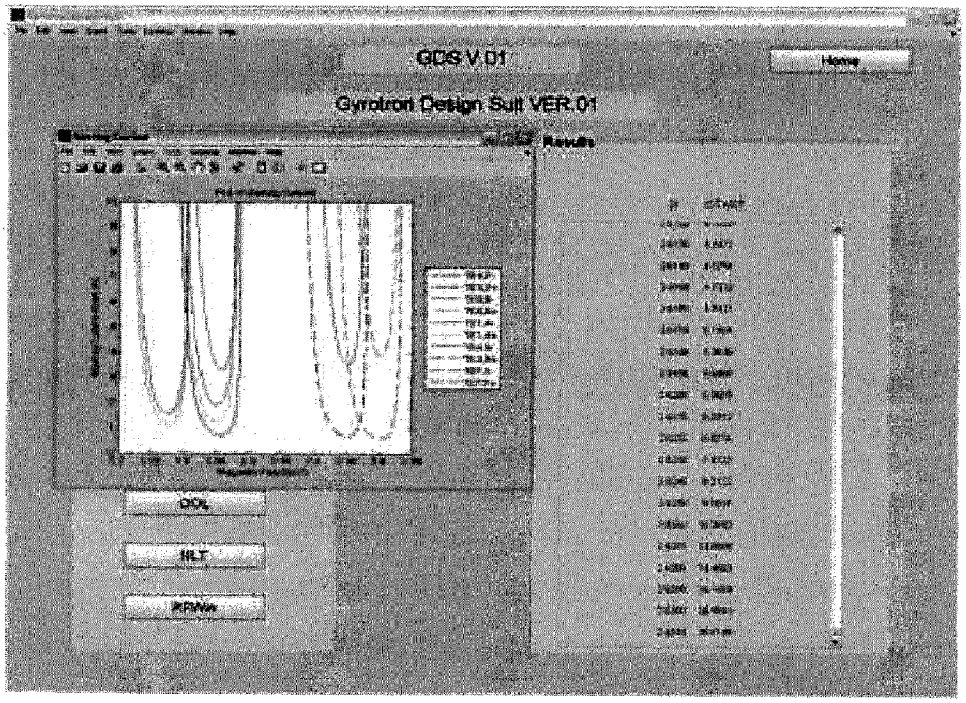

Figure 3.5: Starting Current Computations.

From the plot of the starting currents it can be analyzed easily that whether the candidate mode is well separated from the competing modes or not. The basics of the starting current computations have already been discussed in chapter 2 and the results for the 60 GHz gyrotron have been presented in section 4.2.

3.3 Gun Syn (Gun Synthesis)

In this procedure the Baird's tradeoff equations [38] are solved in adiabatic approximation to calculate the design parameters of a Magnetron Injection Gun. The parameters such as magnetic field at the gun, cathode–anode spacing etc. are calculated. The snapshots for the *Gun Syn* procedure are shown for the input file mode in Fig. 3.6 and the user input mode in Fig. 3.7.

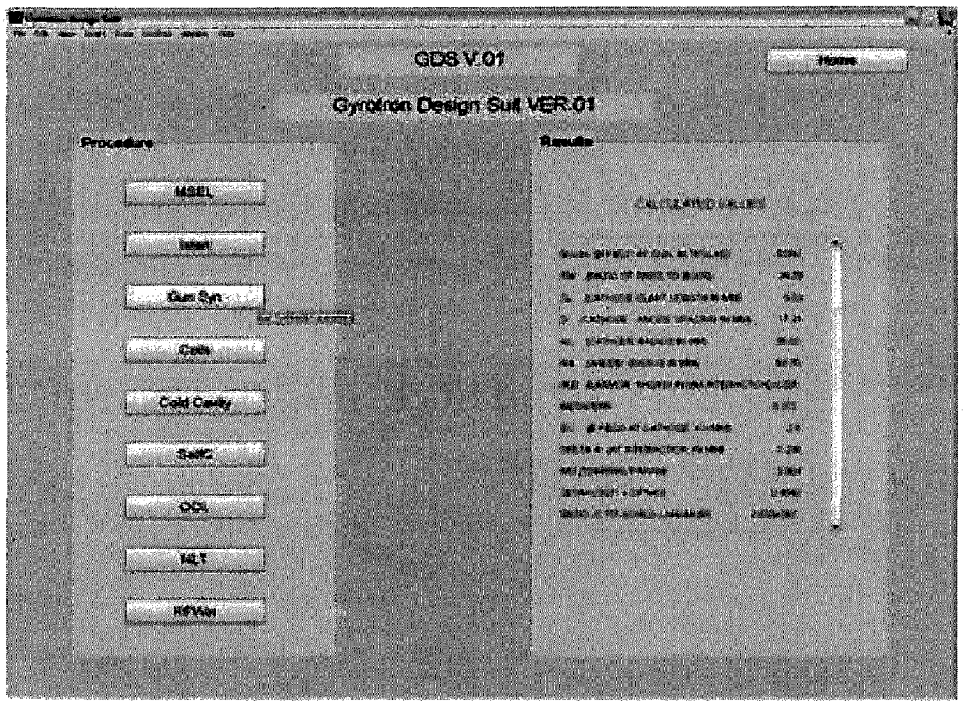

Figure 3.6: Gun Synthesis with Input File.

The output values of the *Gun Syn* are used to make the geometry file of the MIG. The design of a gun requires the use of numerical simulation in rather complicated geometries with non–uniform magnetic fields. The numerical codes are used to optimize the electrode shapes and other gun parameters for the desired electron optical system and beam properties. This is not a part of this software. The design has been separately done using ESRAY code [39] and the results are given in section 4.3.

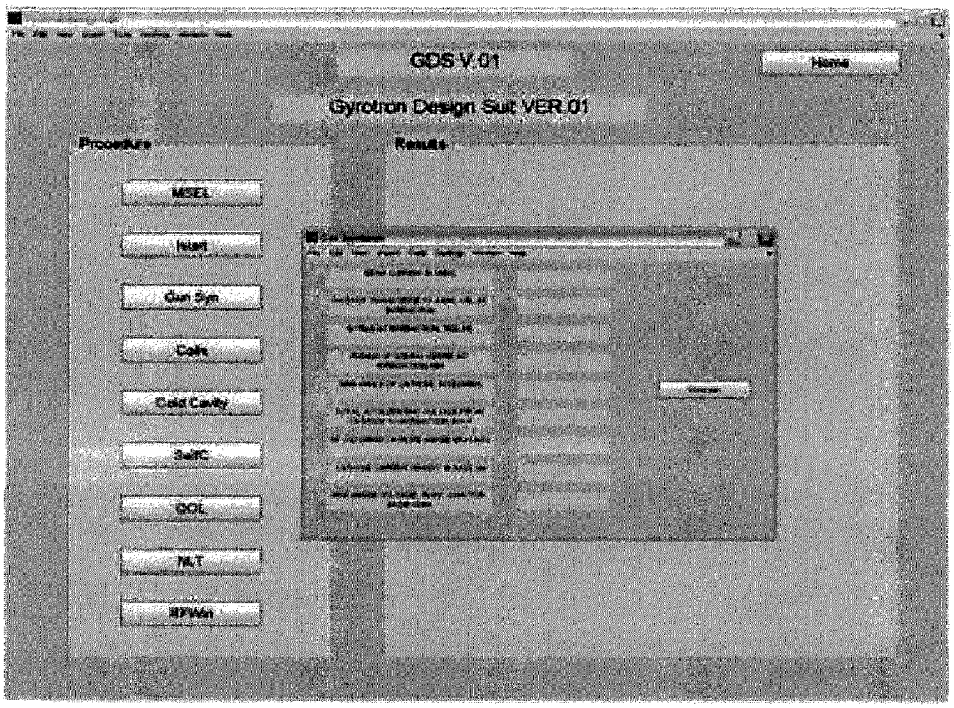

Figure 3.7: Gun Synthesis with User Input.

3.4 Coils (Coil Design)

Gyrotrons mainly employ solenoids which may be either superconducting or normal conducting coils, to provide the necessary magnetic field for beam guidance from the cathode through the interaction region up to the collector. The magnetic guidance system for the gyrotron is designed by designing the coils of the magnets. A current carrying loop produces a magnetic field (Ampere's law) which forms the basis for the design of solenoids.

The magnetic field lines guide the passage and exit of the electrons. The magnetic field is required to be uniform over the resonator with the maximum value at the center of the cavity. By changing the coil dimensions, number of turns and other such parameters the magnetic field can be varied. The *Coils* button calculates the magnetic field over the axial direction and generates a plot of the same on the basis of [4] and [40]. This is shown in Fig. 3.8. The results obtained after coil design for

the specific gyrotron under discussion have been presented in section 4.3.

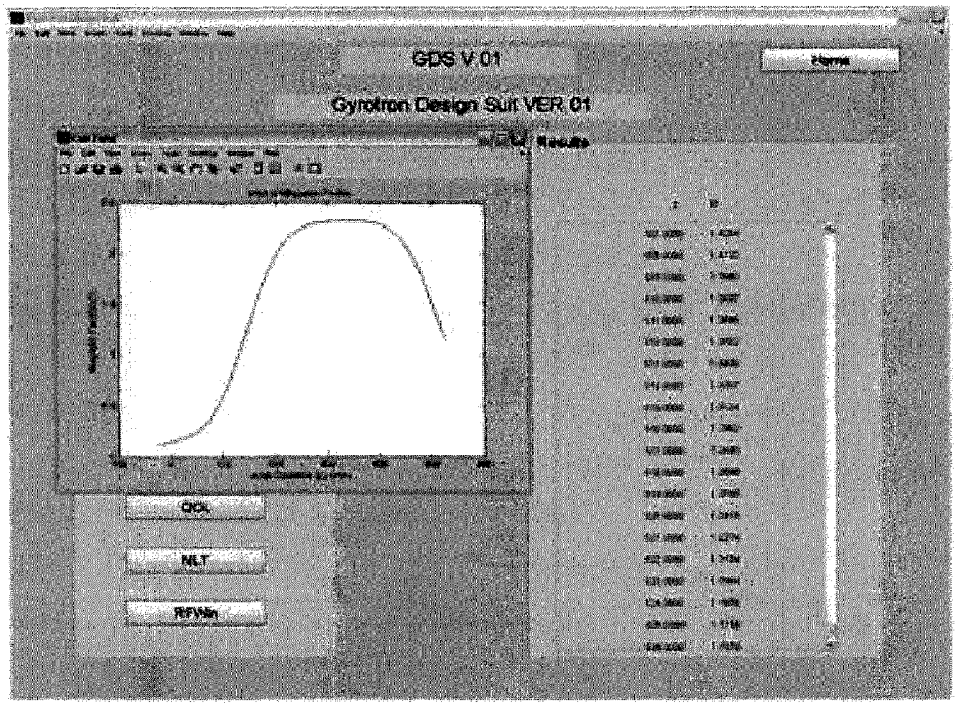

Figure 3.8: Coil Design.

3.5 Cold Cavity

The initial design of the resonator cavity is obtained by carrying out cold–cavity calculations. In these calculations, the adiabatic approximation to equation of electron motion is derived and this equation of motion is solved in the fixed field approximation to compute the efficiency. This module of the software calculates the field profile and the cavity radius with respect to the axial direction following [4, 23, 41, 42]. A plot of the field profile and cavity radius with respect to the z axis is also generated as shown in Fig. 3.9. The user input mode is shown in Fig. 3.10.

The physics of the cold cavity design computations has been described in chapter 2. The output of these cold cavity calculations is further used in self–consistent

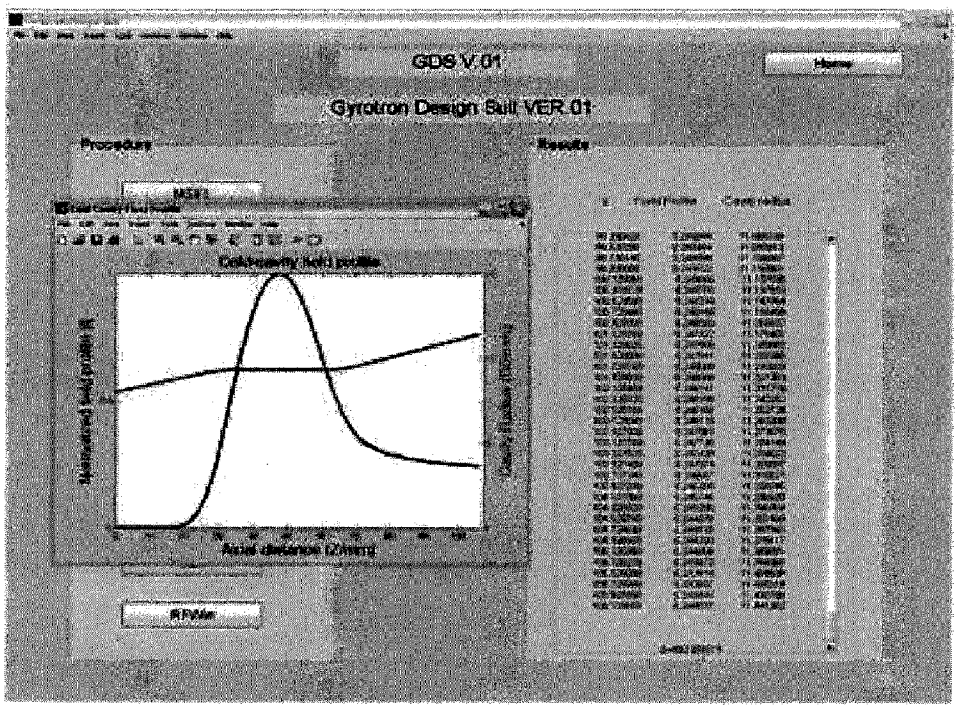

Figure 3.9: Cold cavity design with Input File.

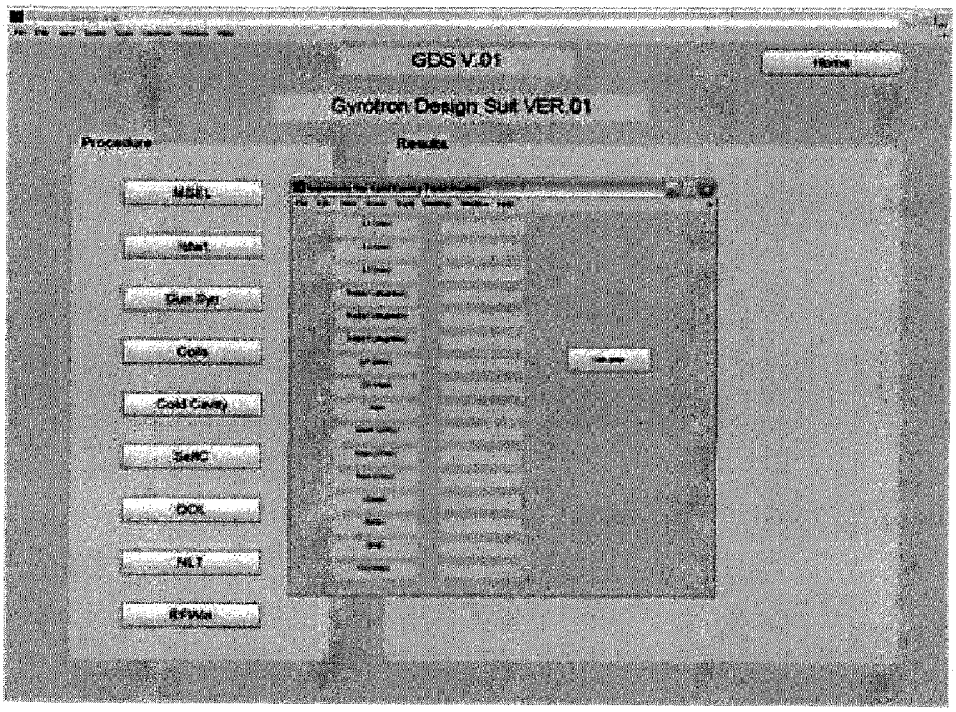

Figure 3.10: Cold cavity design with User Input.

computations to evaluate power and efficiencies. The results of cold cavity design of a conventional cavity gyrotron at a frequency of 60 GHz have been presented in section 4.4.1.

3.6 SelfC (Self–consistent Calculation)

The first approximation obtained by cold cavity calculations must be extended to include the effect of the beam on the cavity field. Thus the equation of motion and wave equations are solved simultaneously to reach a self–consistent solution in a dynamic system which takes into account the effects of the beam on the cavity field profile. The *SelfC* button does the self–consistent calculations following [4,23,24,43]. The results appear as shown in Fig. 3.11.

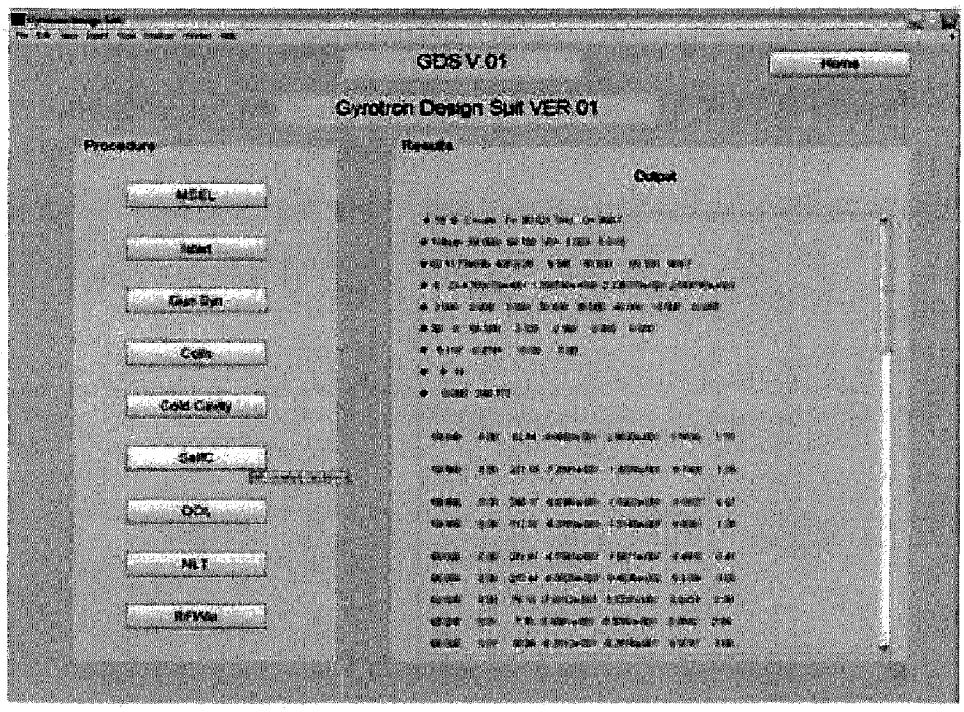

Figure 3.11: Self–consistent Calculations.

There are different self–consistent models for the gyrotrons. The model used here

computes resonant frequency, Q and field profile in Vlasov approximation. This version writes self consistent field profiles, cavity geometry, magnetic field and beam parameters to file for further use by other programs, such as exact solution of equation of motion or mode competition.

3.7 QOL (Quasi–optical Launcher)

High power gyrotrons operate in low–loss volume modes with a high–order mode index. These gyrotron cavity modes are not suitable for power transmission in free space due to their strong diffraction and polarization losses. For long–pulse high power gyrotrons the implementation of an output coupler is required that separates the spent electron beam from the outgoing RF power in order to increase the electron beam interception area of the collector. The preferred output mode of the gyrotron is the fundamental Gaussian beam TEM_{00}. Therefore, a special quasi–optical (q.o.) mode converter is required for the mode conversion from the cavity mode to the eigenwave of the transmission line.

The code behind this button (*QOL*) has been developed to calculate the deformation values for advanced dimpled–wall launcher on the basis of the analysis given by Hirata [29]. The launcher and mode specifications are required as input for this code as shown in Fig. 3.13. The results obtained are as shown in Fig. 3.12. These deformation values are further used to write the surface files (.zfg files). These files are the input files to the Launcher Optimization Tool (LOT) [44] which is used to design the Q.O. Launcher. The results of LOT have been shown in section 4.5.2.

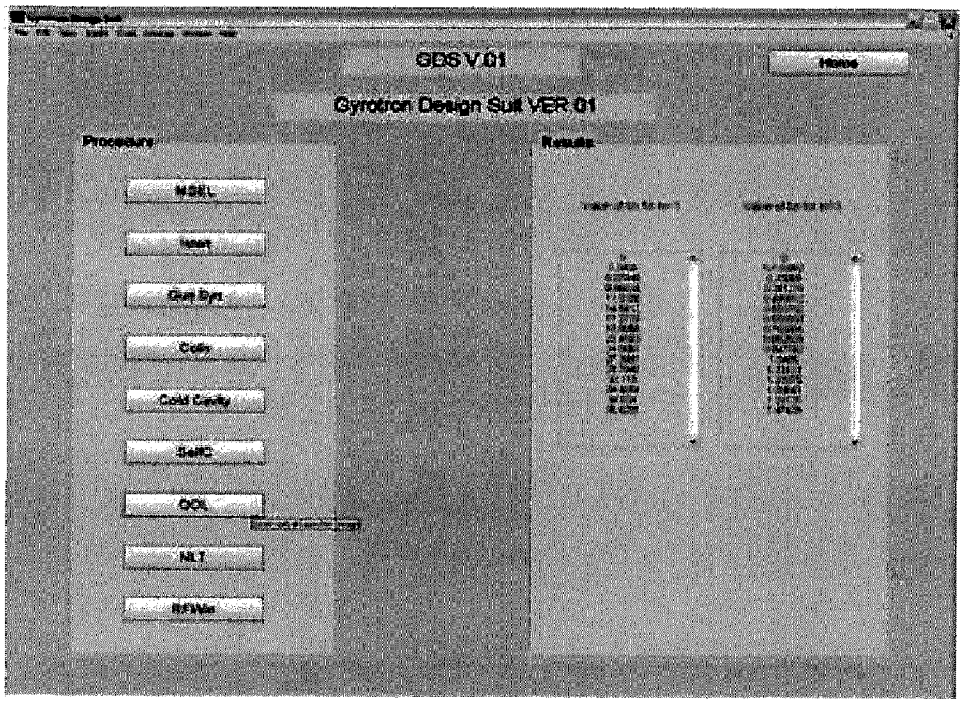

Figure 3.12: Quasi–optical Launcher design with Input File.

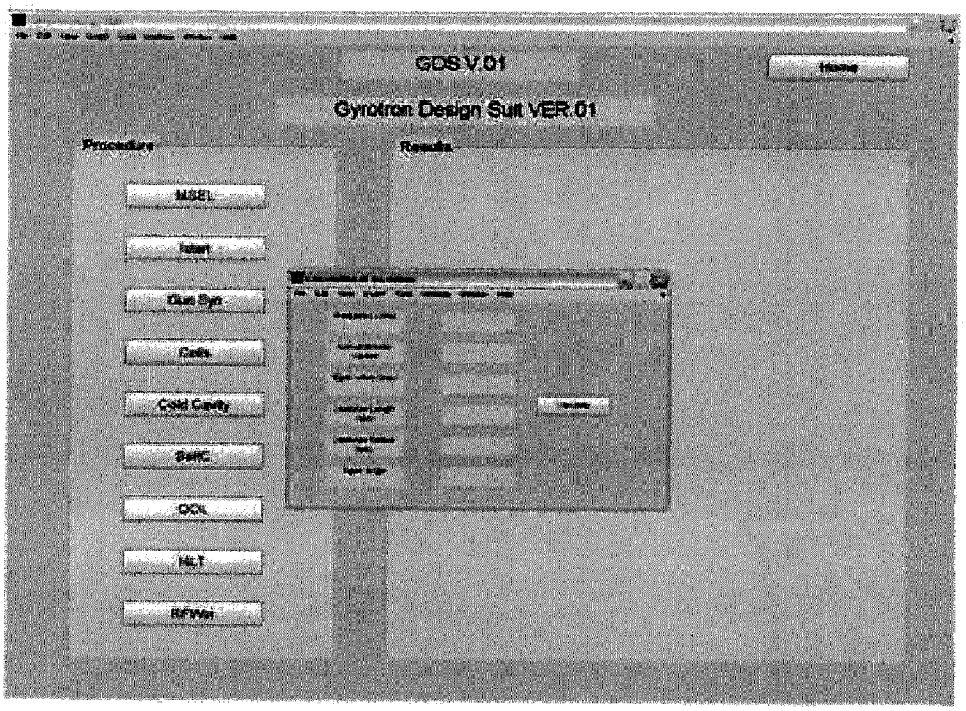

Figure 3.13: Quasi–optical Launcher design with User Input.

3.8 NLT (Non–linear Taper)

Even when the desired mode is produced, mode competition and other considerations often demand waveguide dimensions that are incompatible with the heat load requirements of the beam dump or the electric field constraints on the output window. To meet these constraints, a slowly varying waveguide cross section after the interaction circuit is usually favored over a discrete transition because of transmission and mode purity considerations.

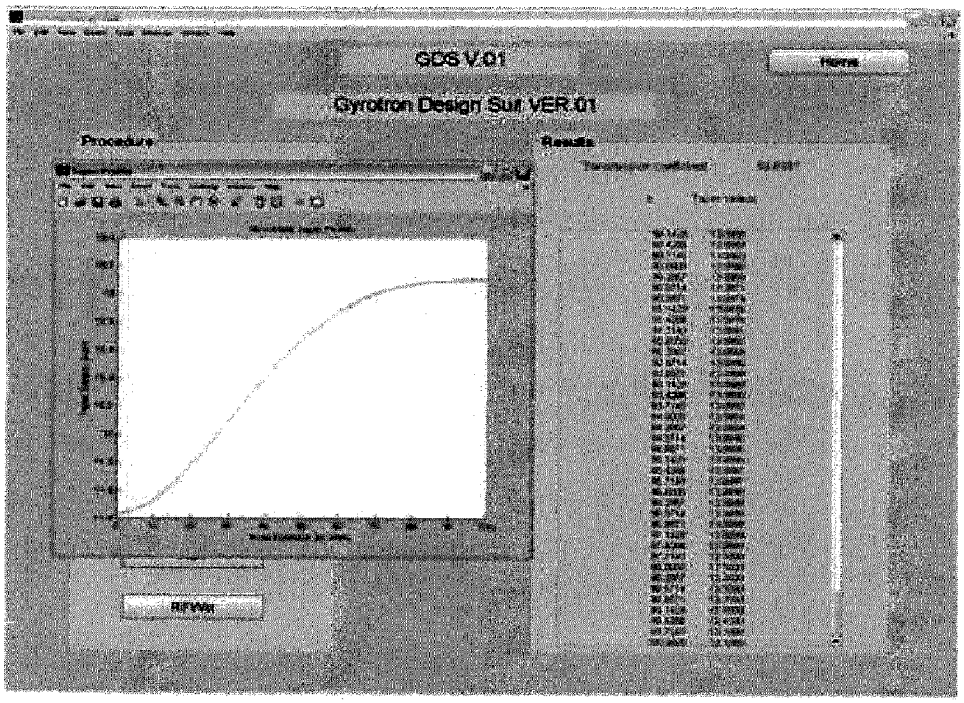

Figure 3.14: Non–linear Taper design with Input File.

The button *NLT* runs the design code of non-linear taper following Wagner [28], and gives the transmission coefficient value for the taper specifications. It also generates the taper profile as shown in Figs. 3.14 and 3.15. Raised–cosine profile taper has been generated. The values of the taper radius with respect to the axial distance from which the profile has been generated are shown in the *Results* panel. Taper design results for 60 GHz have been presented in section 4.5.1.

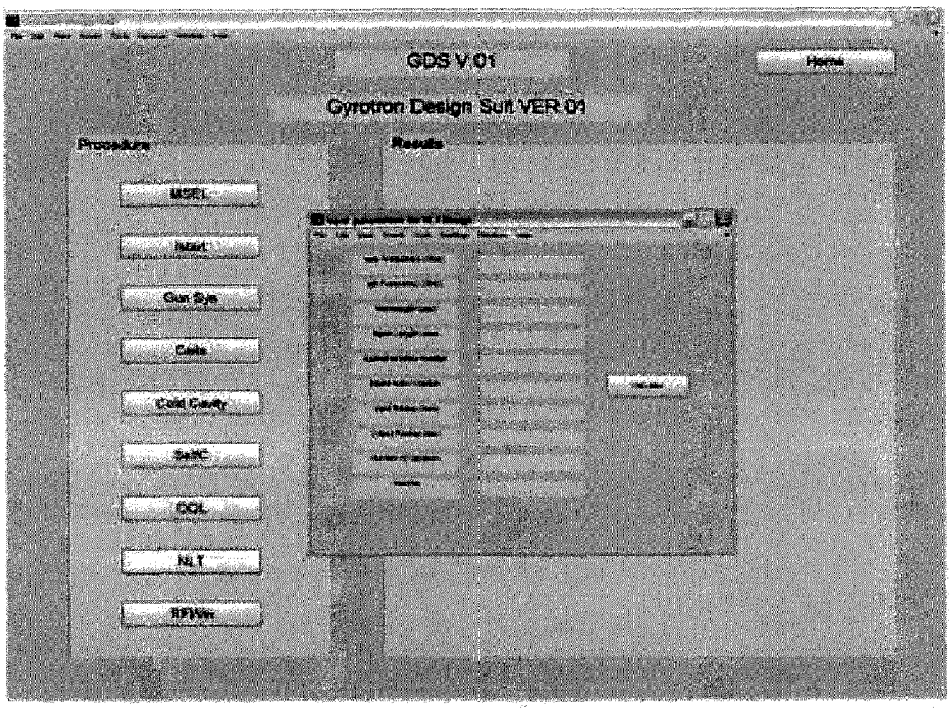

Figure 3.15: Non–linear Taper design with User Input.

3.9 RFWin (RF–Window)

When this button is clicked a separate GUI window appears as shown in Fig. 3.16. It is complete in itself for the design of any single disc or double disc window following Nickel in [45]. Different panels are present for specifying the input parameters such as the RF parameters, the disc specifications, the material specifications and coolant parameters.

In the output the absorption, reflection, transmission and VSWR values are generated with respect to the frequency. The optimum frequency value is also selected and shown. The reflection (S_{11}) and transmission (S_{21}) can also be plotted with respect to frequency. The snapshot of the GUI with results is shown in Fig. 3.17. The results of the design of double disc window for 60 GHz have been shown in section 4.5.3.

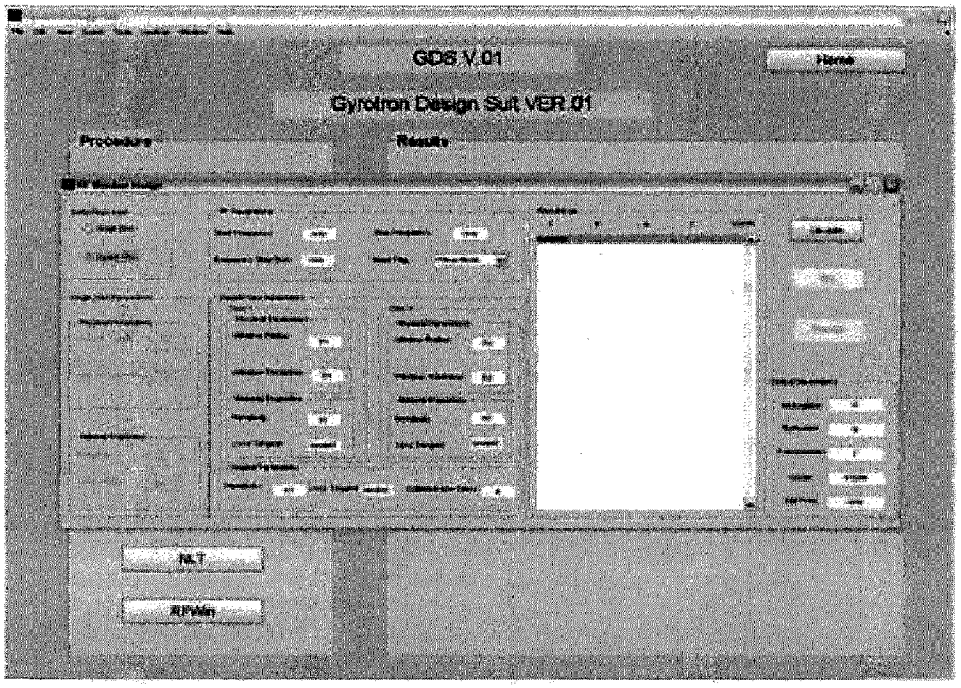

Figure 3.16: RF Window Design.

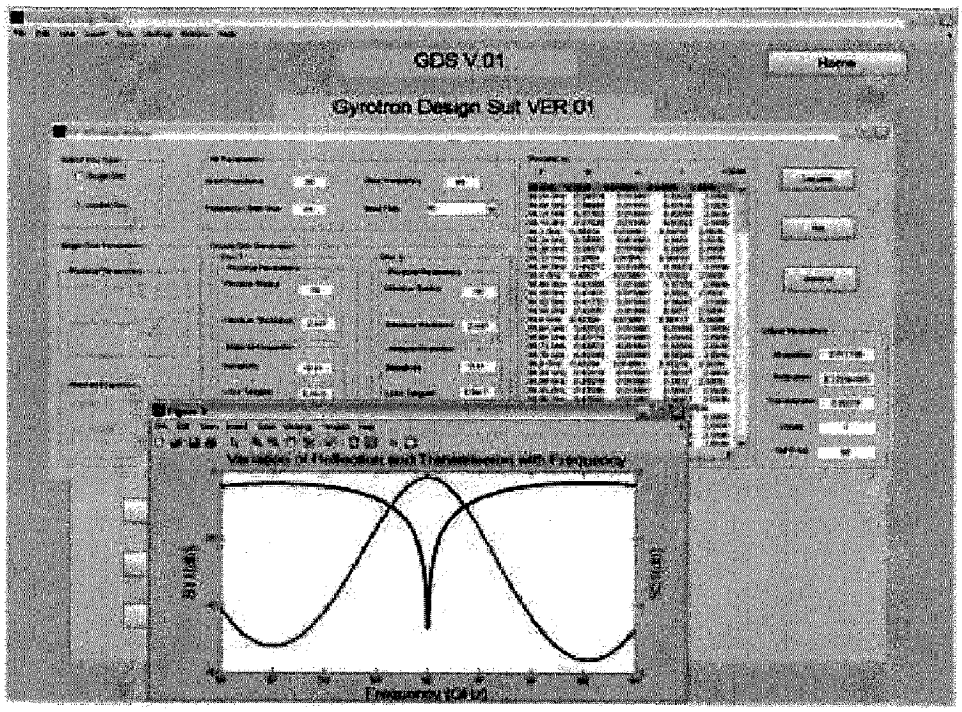

Figure 3.17: RF Window Design GUI with results.

Chapter 4

Design Studies

In this chapter the design studies of the specific gyrotron have been illustrated along with the results obtained. The design parameters and goals for this 60 GHz, 100 kW CW conventional cavity gyrotron are as stated in Table 4.1.

Table 4.1: Design Parameters and Goals.

Frequency	60	GHz
Output power	≈100	kW, CW
Diffraction Q (Q_D)	≈ 1000	
Beam current (I_b)	5 – 10	A
Accelerating voltage (U_b)	60 – 70	keV
Magnetic field (interaction)	≈ 2.1–2.3	T
Velocity ratio (α)	≈ 1.3	
Total output efficiency	≈ 35	%
Estimated wall losses	< 2.0	kW/cm^2
Overall losses	< 10	%

4.1 Mode Selection

The given frequency corresponds to a free–space wavelength of 5 mm. As we very well know, the electromagnetic radiation in a gyrotron is produced in a TE mode near the cutoff frequency for that mode. For operation in the $TE_{m,p}$ mode, the cavity radius is related to λ by $R_0 = \chi_{m,p}\lambda/(2\pi)$ where $\chi_{m,p}$ is the p^{th} root of $J'_m(\chi)$=0. For operation at the first harmonic (s=1) the optimum electron beam radius is given by $R_b = \chi_{m\pm1,i}R_0/\chi_{m,p} = \chi_{m\pm1,i}\lambda/(2\pi)$, (i=1 or 2). In general, the co–rotating mode (with the lower sign) is chosen, since this provides better coupling of the electron beam to the RF–field.

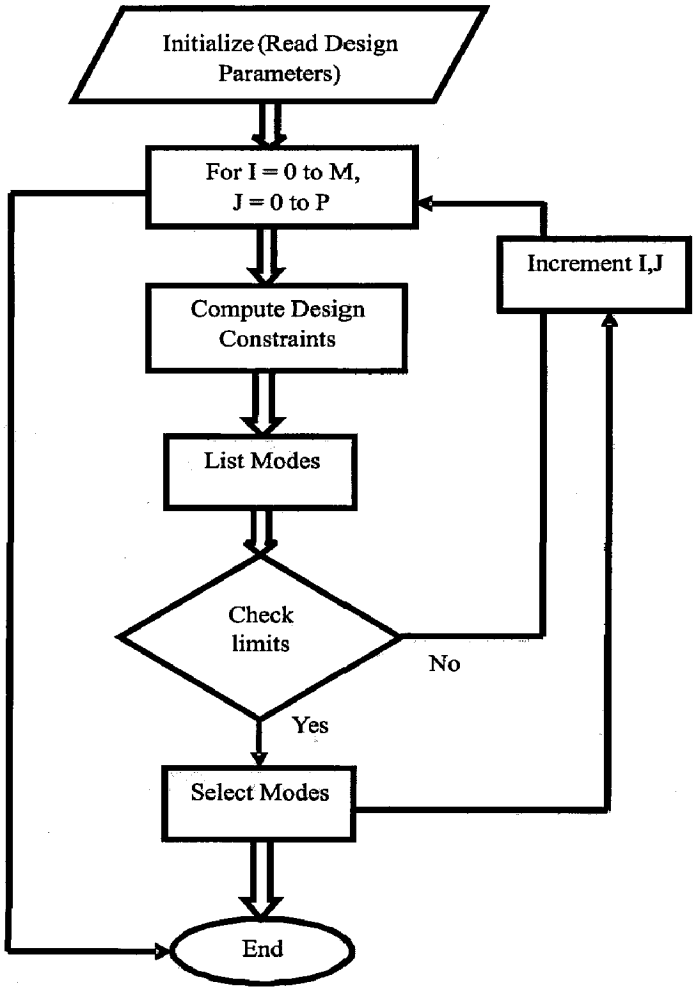

Figure 4.1: Methodology of Mode Selection Procedure.

In the mode selection procedure, all the modes with eigenvalues ranging from 8 to 18 were inspected (as matter of experience). In addition to the satisfactory evaluation of the modes that are meeting the general design considerations (such as peak wall loading, voltage depression, limiting current, etc.), the candidate modes should also support an advanced dimpled wall launcher of the quasi–optical output coupler. These design constraints have been explained earlier in chapter 2 and constraint limits are given in Table 2.1. Only well qualified modes are selected for this feasibility study. The general methodology of mode selection has been depicted in the flowchart in Fig. 4.1.

Table 4.2: Azimuthal index, radial index, mode eigenvalue, cavity radius, beam radius, voltage depression, limiting current, peak–wall loading, and $m_2/2$ $(= 360°/\phi)$ for probable candidate modes for a 60 GHz gyrotron.

m	p	$\chi_{m,p}$	R_0 mm	R_b mm	V_d kV	I_L A	dP/dA kW/cm^2	$m_2/2$
0	3	10.173469	8.10	1.47	1.88	23.7	.060	2.00
3	2	8.015237	6.38	2.43	1.06	42.0	.113	2.65
3	3	11.345925	9.03	2.43	1.45	30.9	.052	2.41
4	2	9.282396	7.39	3.34	.87	51.1	.089	2.79
4	3	12.681909	10.09	3.34	1.22	36.7	.043	2.51
5	2	10.519861	8.37	4.23	.75	59.4	.073	2.92
6	2	11.734936	9.34	5.11	.67	67.1	.061	3.04
7	2	12.932386	10.29	5.97	.60	74.4	.053	3.15

The values of the design constraints of each of these modes are calculated as shown in Table 4.2. Three modes, namely $TE_{5,2}$, $TE_{6,2}$ and $TE_{7,2}$, were found to be within the design constraints. But to fulfill the requirements of the advanced dimpled–wall quasi–optical launcher, $TE_{6,2}$ mode was found to be the best candidate.

4.2 Mode Competition and Starting Currents

As a next step, the starting currents have been computed for this candidate mode and possible competing modes that might prevent operation in the desired mode. The starting currents for a $TE_{6,2}$ mode gyrotron operating at 60 GHz along with its competing modes is shown in Fig. 4.3. A Gaussian field profile was employed for these calculations, which is a common practice to initially compute the starting currents of main mode and its competitors to have a preliminary assessment. The general methodology of starting current computation has been depicted in the flowchart in Fig. 4.2.

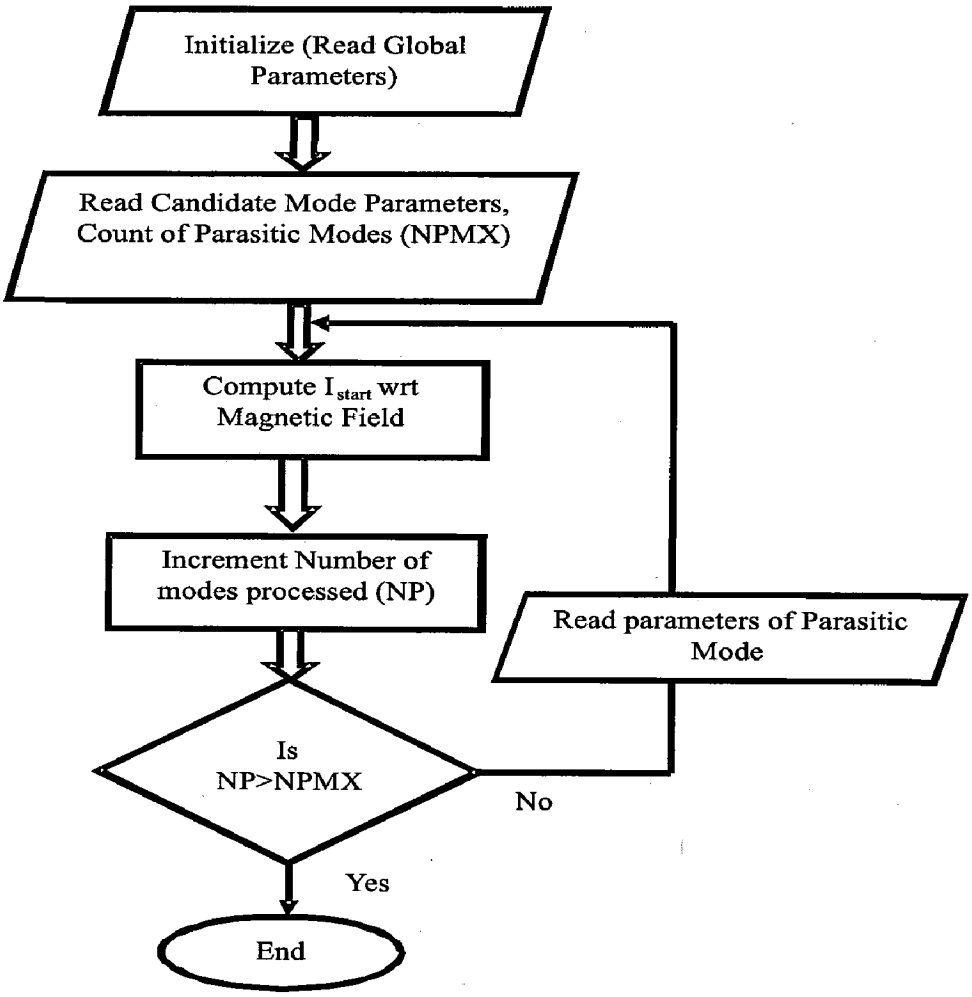

Figure 4.2: Methodology of Starting Current Computation.

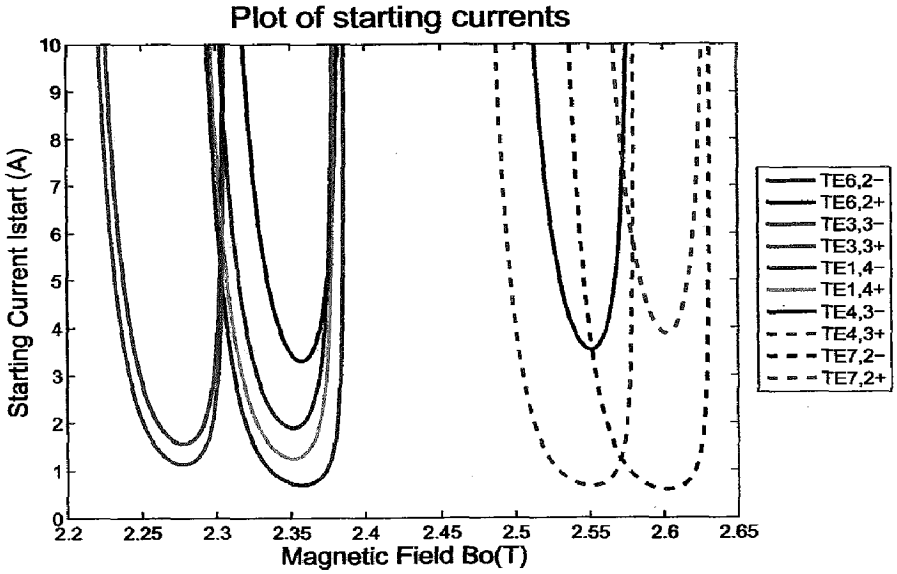

Figure 4.3: Starting current I_{start} as a function of magnetic field B_0 for various modes with beam radius (R_b) optimized for the $TE_{6,2}$ mode at 60 GHz, with accelerating voltage $U_0 = 65$ kV, $\alpha = 1.3$, $R_0 = 9.34$ mm, $R_b = 5.11$ mm, and $Q_D = 954$.

By inspection of the starting current curves that were computed for the candidate mode and possible competing modes, as shown in Fig. 4.3, it became clear that the $TE_{6,2}$ mode was best separated from possible competing modes. Also during the mode selection process it has been observed that this mode satisfies all technical design constraints within the limits. Hence this mode has been considered as operating mode for further studies.

4.3 MIG and Guidance System

Electron optical and guidance systems namely, the magnetic coils and electron gun are major components of a gyrotron oscillator. In this section, the design of the magnetic coil systems and magnetron injection gun has been carried out.

4.3.1 Magnetic Guidance System

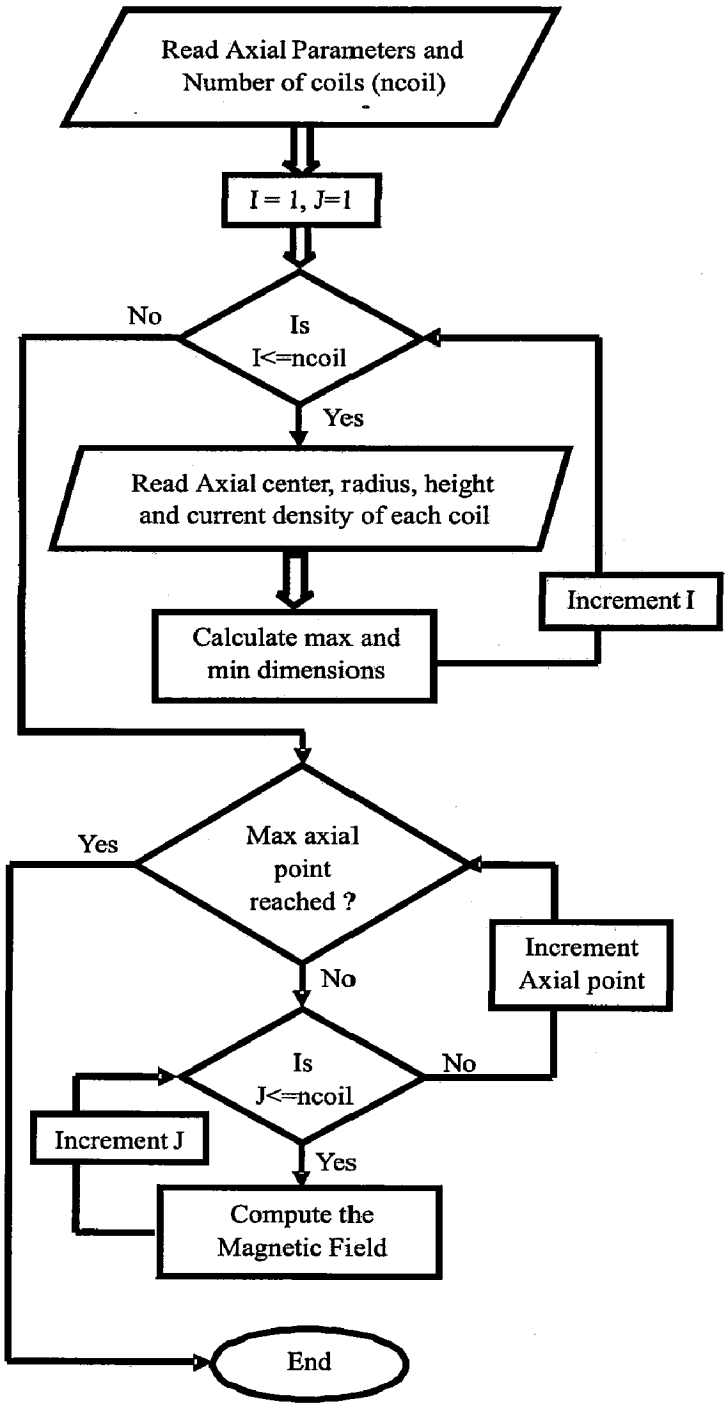

Figure 4.4: Methodology of Guidance System Design.

The magnetic guidance system design is a very important step in the design of gyrotrons. A rough estimation of the device length can be made by looking at the magnetic field profile. Magnetic field profile data are needed to perform precise simulation studies on magnetron injection gun and RF–behavioral aspects. In addition, it is required for collector design. Most gyrotrons employ solenoids (either superconducting or normal conducting coils) to provide necessary magnetic field for beam guidance from the cathode through interaction region up to the collector. In this section, the design of a magnetic guidance system required for a 60 GHz, 100 kW, CW gyrotron is presented. The general methodology undertaken to design the coils has been depicted in the flowchart in Fig. 4.4.

Table 4.3: Coil Data.

Coil	ΔZ (mm)	ΔR (mm)	N_C	I_C (A)
Main Coil	360.00	15.00	9920	72
Aux Coil – 1	90.00	7.50	630	72
Aux Coil – 2	90.00	7.50	630	72
Gun Coil	20.00	15.00	610	-49.5

A simple and cost effective magnet design can be achieved using a single coil which gives the maximum required field at the center of the cavity and uses the stray field in the gun and collector region. However, in a more effective design of the magnetic guidance system employed here, a single main coil, two auxiliary coils and one gun coil have been used. The coil data has been calculated using GDS and shown in Table 4.3. The plot of the magnetic profile generated by GDS is shown in Fig. 4.5. This initial data is then optimized using ESRAY. The axial magnetic field with the proposed coil arrangement with gun geometry and a plot of magnetic flux lines obtained through ESRAY are shown in Figs. 4.6 and 4.7. A magnetic field of 2.32 T is obtained over the uniform section of the cavity. The center of the cavity is

situated at 338 mm from the cathode.

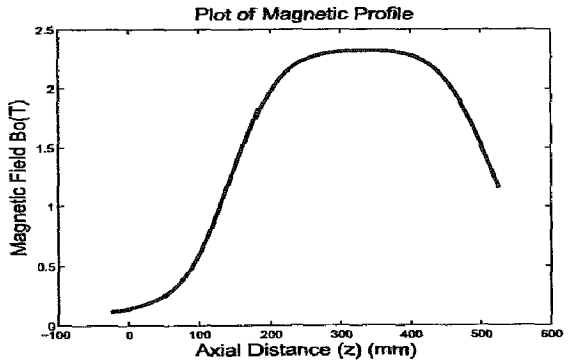

Figure 4.5: Magnetic field profile of the coils obtained through *GDS*.

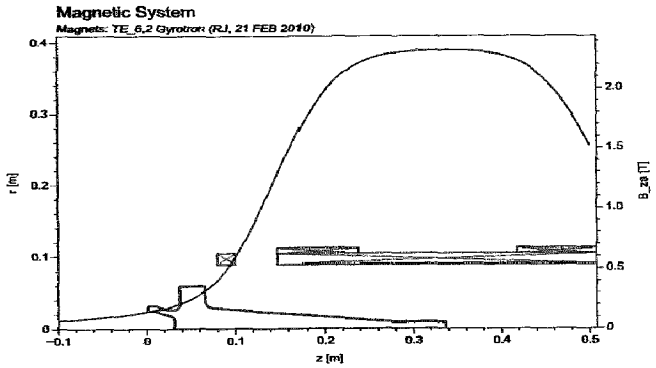

Figure 4.6: Magnetic field profile of coils through *ESRAY* [39].

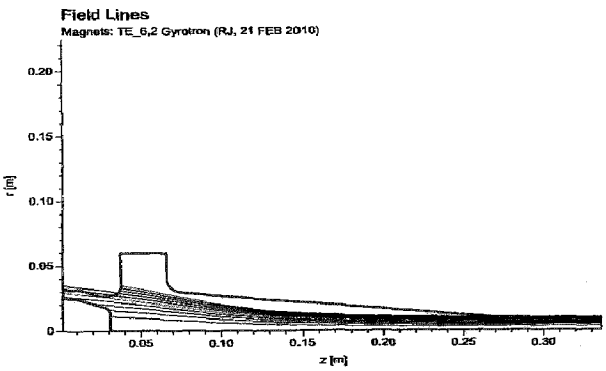

Figure 4.7: Plot of magnetic flux lines using ESRAY [39].

4.3.2 Magnetron Injection Gun

For the $TE_{6,2}$ mode operating at the first harmonic, the beam radius is 5.11 mm. Assuming a compression ratio of approximately 18, gives a cathode radius of approximately 21.5 mm. The accelerating voltage should be in the range 65–70 kV, and the velocity ratio approximately 1.2–1.4. Simple adiabatic theory, leading to the Baird–Lawson equations [38] indicates that, for a triode-type gun, and parameters as given above, the anode-cathode spacing would be rather large. Under adiabatic approximation, the electron motion in crossed electric and magnetic fields can be separated into a gyration motion of the electrons and a drift of their guiding centers [4]. This adiabatic approximation is valid if the electric and magnetic fields are rather small at dimensions characteristic for the electron trajectories.

Table 4.4: Design Data of Triode Type MIG.

Beam current	5–10	A
Accelerating voltage	≈ 67	kV
Compression ratio	18	
Beam radius (interaction)	5.11	mm
Larmor radius (interaction)	0.308	mm
Cathode radius	21.02	mm
Cathode angle	20.8	°
Anode angle	20.8	°
Cathode slant length	3.52	mm
Emitter current density	2.1	A/cm^2
Cathode-anode clearance	9.77	mm
Velocity ratio α	1.2–1.4	
Electric field at cathode	4.2	kV/mm

As a matter of convenience and flexibility, a triode version of the MIG has been

proposed. In addition, it provides more possibilities to control beam parameters. However, a diode type MIG is simpler to realize. Assuming a compression ratio of about 18, the design data have been prepared and are shown in Table 4.4. The initial design was obtained following a simple adiabatic theory, following the Baird–Lawson equations [38]. The design is then refined using the ESRAY code [39].

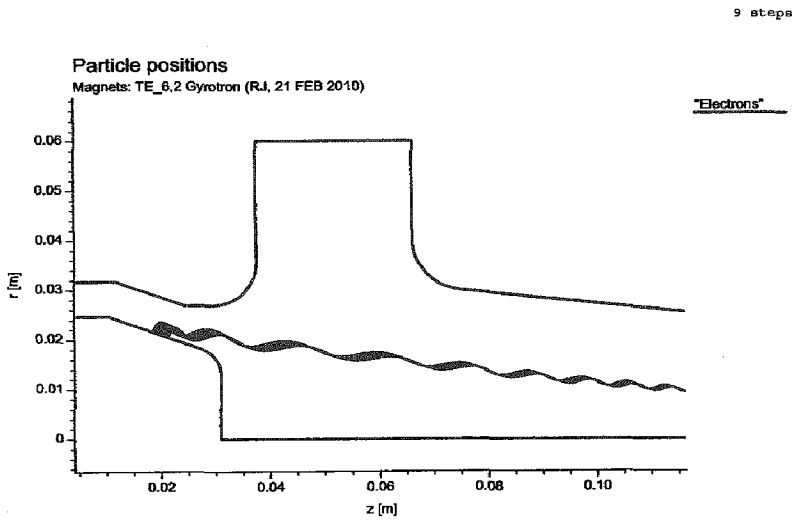

Figure 4.8: Triode type MIG with particle trajectories [39].

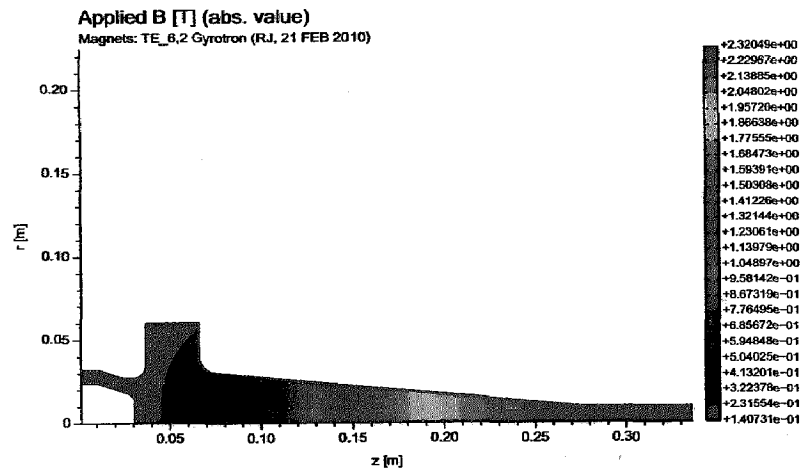

Figure 4.9: Contours of the magnetic field in the MIG region [39].

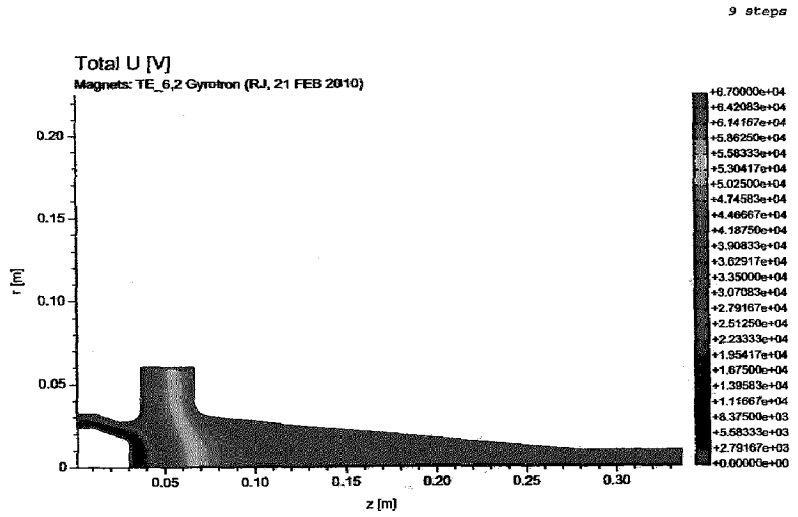

Figure 4.10: Contours of the total voltage in the MIG region [39].

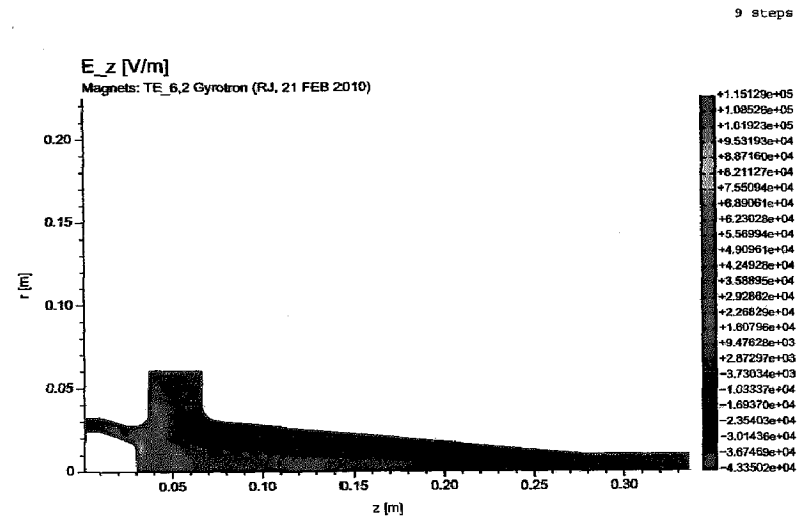

Figure 4.11: Contours of E_z in the MIG region [39].

Fig. 4.8 shows the geometry of the gun and the particle trajectories for one of the optimized runs of ESRAY. Typical beam properties obtained for a compression of b = 18 are fairly good and are U_b = 66.06 kV, α = 1.2925, $\beta_\perp$ = 0.367, $\Delta\alpha/\alpha$ = 5.788%, with U_{mod} = 34.0 kV and I_b = 10 A. It is noted that the velocity spread increases significantly for higher values of U_{mod}, mainly due to the larger values of $\beta_\perp$ for electrons emitted from the outside edges of the emitter. Figures 4.8–4.11 show the results obtained by the ESRAY simulations.

4.4 RF Behavior

The optimum cavity design is carried out by computing the power and interaction efficiencies in cold cavity and self–consistent approximations for various parameters until a satisfactory cavity design compatible with the design goals such as efficiency, wall losses, output power etc. is obtained.

4.4.1 Cold-cavity Design Calculations

The cavity is a standard three section structure with an input taper and a uniform mid–section followed by an output uptaper. The beam–wave interaction takes place in the uniform mid–section where the RF–fields reach peak values. The external magnetic field starts to decrease in the uptaper region which results in residual interaction that sometimes causes a loss of efficiency. Therefore the output taper has not been included as a part of resonator geometry. The methodology undertaken for the cold cavity analysis has been portrayed through a flowchart in Fig. 4.12.

Table 4.5 shows the different sets of cavity data for which computations have been carried out. For the $TE_{6,2}$ mode at 60 GHz, the cavity radius is 9.34 mm and beam radius is 5.11 mm. For cavities with moderate quality factors, the length parameter of the Gaussian field profile L is generally taken between $7\lambda \leq L \leq 8\lambda$, where λ is the free space wavelength. As the wavelength is 5 mm, it gives a diffractive quality

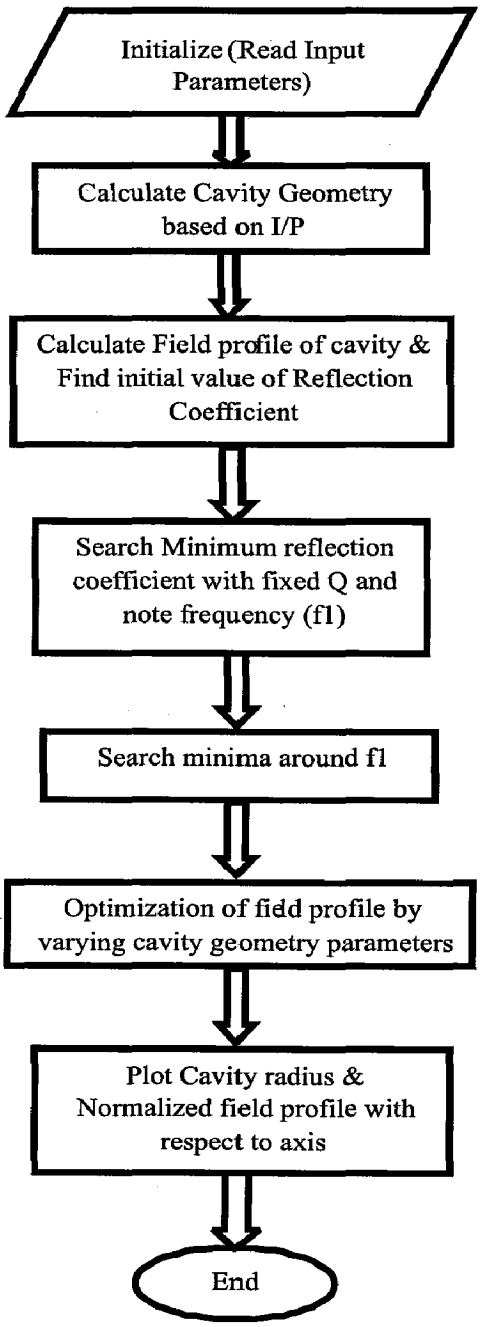

Figure 4.12: Methodology of Cold-cavity Design Calculations.

Table 4.5: Interaction cavity data.

	Set # 1	Set # 2	Set # 3	Set # 4	Set # 5
L_1 (mm)	30	30	30	30	30
L_2 (mm)	34	35	36	37	38
L_3 (mm)	40	40	40	40	40
θ_1 (°)	2.5	2.5	2.5	2.5	2.5
θ_2 (°)	0.0	0.0	0.0	0.0	0.0
θ_3 (°)	3.0	3.0	3.0	3.0	3.0
D_1 (mm)	10.0	10.0	10.0	10.0	10.0
D_2 (mm)	10.0	10.0	10.0	10.0	10.0
f GHz	60.029	60.024	60.019	60.015	60.011
Q_D	825	888	954	1023	1095

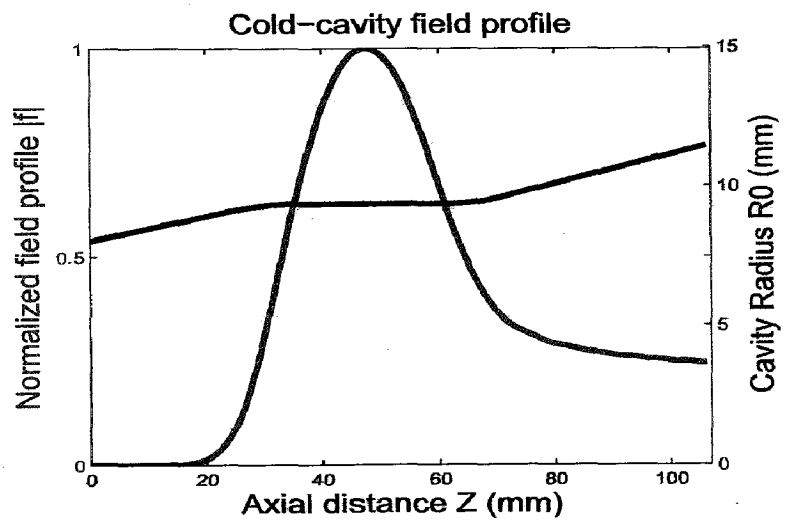

Figure 4.13: Final Cold-cavity Field Profile.

Table 4.6: Final Design of the Cold–Cavity.

R_1	8.03	mm
R_2	9.34	mm
R_3	11.436	mm
L_1	30	mm
L_2	36	mm
L_3	40	mm
θ_1	2.5	°
θ_2	0	°
θ_3	3.0	°
D_1	10	mm
D_2	10	mm
Q_{Diff}	954	

factor $Q_D \approx 900$. We have varied the cavity mid–section length over the range and obtained the data as shown in Table 4.5. After a careful study of the various sets of results obtained keeping in mind the goals defined, a cavity mid–section length of 36 mm was selected as it gives a $Q_D = 954$. The wall losses become too high for greater quality factors. The final cavity data has been depicted in Table 4.6. Fig. 4.13 shows the cold–cavity field profile, as well as the cavity geometry for $L_2 =$ 36 mm. The output of these cold cavity calculations is further used in self–consistent computations to evaluate power and efficiency.

4.4.2 Self-consistent Calculations

Self–consistent calculations [4,23] for power and efficiency are carried out for a range of external parameters, namely: beam energy, beam velocity ratio α, beam current and applied magnetic field. Computations are carried out for three cavity mid–section lengths $L_2 = 34.0/36.0/38.00$ mm that give values of $Q_D = 825/954/1095$

respectively.

The results of the cavity design based on self-consistent computations are shown in Figs. 4.14–4.17. These indicate the cavity geometry corresponding to $Q_D = 954$ as the best choice. From these figures, it is evident that operation at the fundamental (s=1) at 60 GHz with the $TE_{6,2}$ mode as the operating mode gives well above 100 kW of cavity output power with around 38% efficiency and maximum wall losses of 0.5 kW/cm^2.

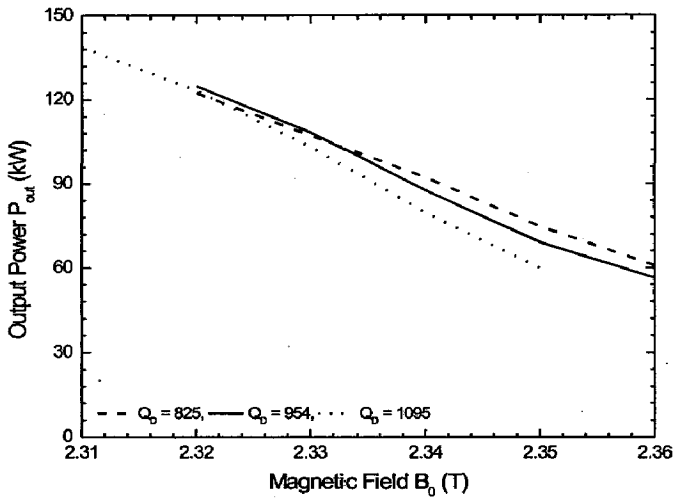

Figure 4.14: Output power as a function of cavity magnetic field (B_0) with: U_B = 65 kV, I_B = 5 A, and α = 1.3.

In addition, time–dependent self–consistent (SELFT) calculations [46] are carried out for various values of Q_D considering all the probable competing modes. Fig. 4.18 shows the results of a simulation with SELFT for the $TE_{6,2}$ mode along with probable competing modes. In these calculations, the beam energy is increased from 40 keV to 65 keV over a fictitious startup time of 5000 ns (typical voltage rise times are around 100 μs), and the velocity ratio varies accordingly. The beam current and magnetic field are held constant. The computations are carried out for three different

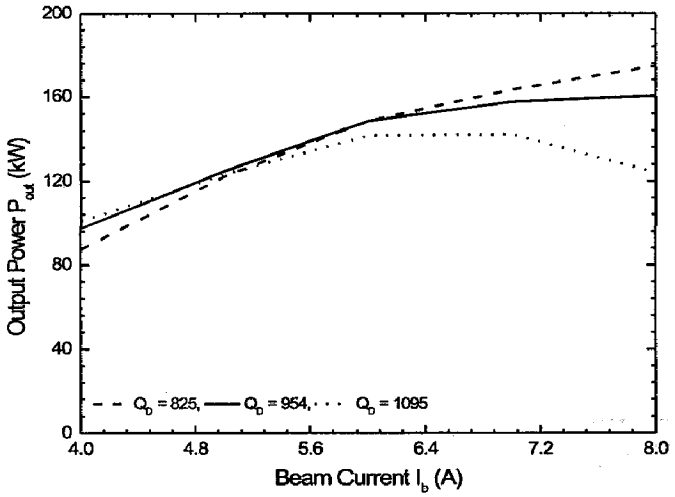

Figure 4.15: Output power as a function of beam current (I_B) with: $U_B = 65$ kV, $B_0 = 2.32$ T, and $\alpha = 1.3$.

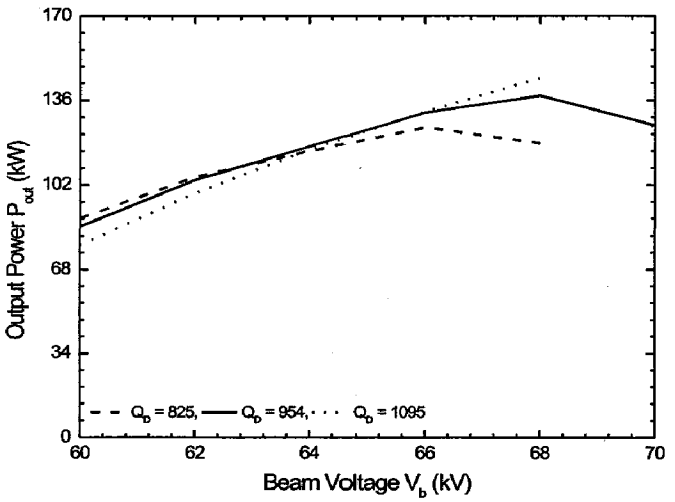

Figure 4.16: Output power as a function of beam voltage (U_B) with: $I_B = 5$ A, $B_0 = 2.32$ T, and $\alpha = 1.3$.

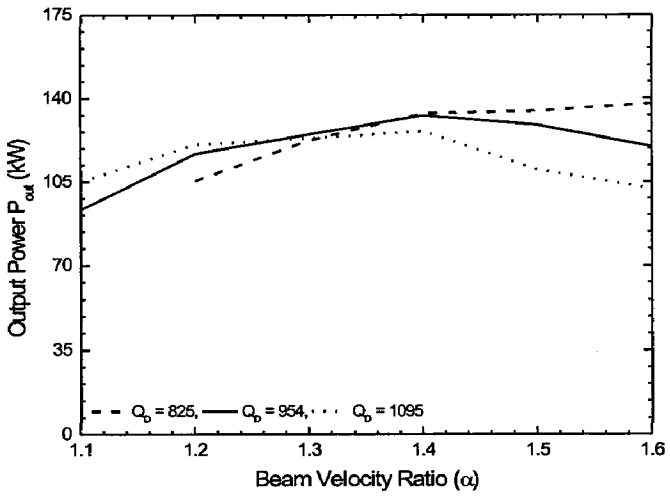

Figure 4.17: Output power as a function of beam velocity ratio (α) with: $U_B = 65$ kV, $I_B = 5$ A, and $B_0 = 2.32$ T.

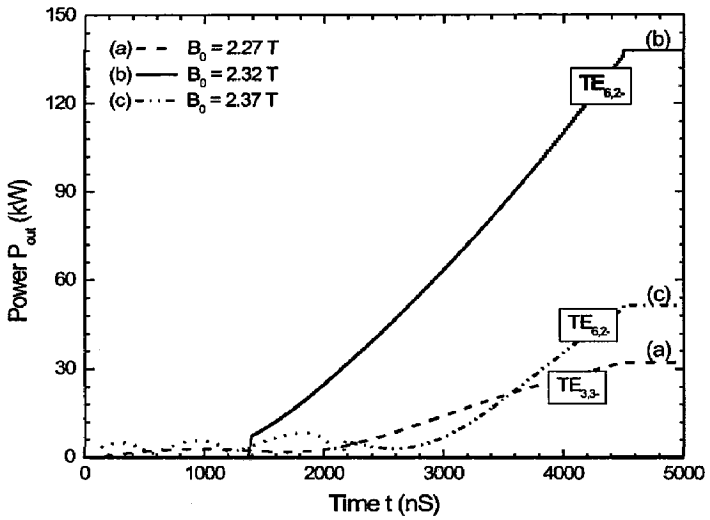

Figure 4.18: SELFT simulation results for a $TE_{6,2}$ gyrotron considering the probable competing modes. (a)$B_0 = 2.27$ T,(b)$B_0 = 2.32$ T and (c)$B_0 = 2.37$ T.

magnetic fields (B_0(T) = 2.27, 2.32, 2.37). If the magnetic field remains constant at 2.32 T, then the $TE_{6,2}$ mode oscillates well. These results indicate that stable operation of a gyrotron in the $TE_{6,2}$ mode at 60 GHz at power levels around 100 kW should be possible.

4.5 Output System

The output system consists of:

a) A Non–linear Taper which connects the interaction region with the main waveguide system.

b) A Quasi–optical Launcher for radial output coupling.

c) RF–Window to transmit power outside the gyrotron.

d) A Collector for the dissipation of the energy of electrons.

In this section these components of the output system have been designed.

4.5.1 Non–linear Taper

The requirement of a diameter taper in gyrotrons is to provide a good match between input and output sections of the taper with very low spurious mode content. In gyrotrons, cross–section taper (in general of cylindrical type) are employed between the output section of the cavity to the main waveguide section. Cross-section tapers should not generate spurious modes above a certain acceptable level.

In this work, a raised cosine taper profile has been used as it yields very low mode conversion [47]. The analysis of the taper was carried out using a dedicated scattering matrix code [28]. The parameters of the non–linear taper are: the length of the taper (L), the radius of the taper at the input end (r_1), the radius of the taper at the output end (r_2), the number of sections to be discredited (N), and a geometrical

Table 4.7: Final Design of Non–linear Taper.

r_1	11.436 mm
r_2	13.100 mm
L	100.00 mm
γ	0.67
N	350
S_{21}	99.6087%

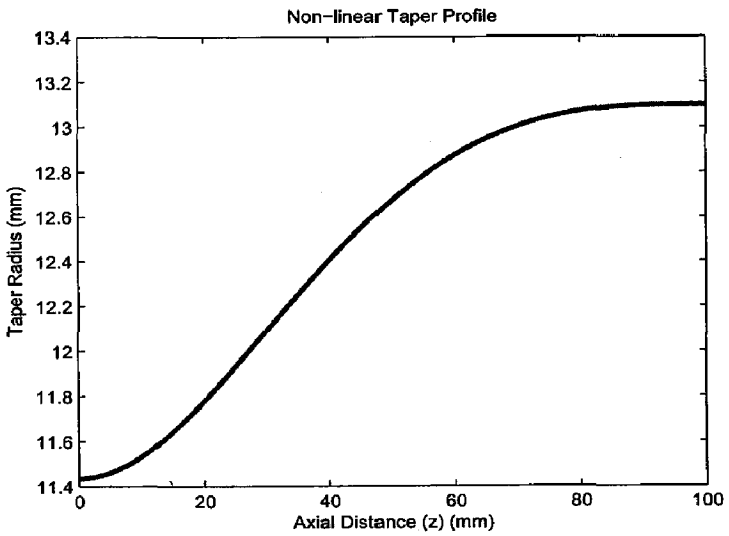

Figure 4.19: Final profile of the designed non–linear taper for the values given in Table 4.7.

parameter gamma (γ). L, N and γ are varied while keeping r_1 and r_2 constant to achieve maximum transmission. The values of the design parameters considered for the design are summarized in Table 4.7. The objective of the design was to obtain a maximum transmission coefficient (i.e. S_{21}–parameter), operating with $TE_{6,2}$ mode with minimized spurious mode content.

Finally, taper contour profile along its length is appreciated graphically in Fig. 4.19. A transmission of 99.6087 % has been obtained. This non-linear taper can further be optimized as given in [48] if required.

4.5.2 Quasi–optical Launcher

The advanced mode converter employs:

- a dimpled–wall waveguide section and a helical-cut launching aperture as an antenna, and
- one quasi–elliptical mirror and two toroidal mirrors as beam–forming mirror system.

The wall distortions (scattering surface) of the dimpled–wall waveguide antenna can transform the input eigenwave to an eigenwave of the weakly perturbed transmission line. That beam is appropriate to be used directly as a free space TEM_{00} mode, or to be transmitted as a low-loss hybrid HE_{11} mode in highly over–moded corrugated waveguide [29, 30, 49].

For the current gyrotron operating at the $TE_{6,2}$ cavity mode the design achieved 99.60 % conversion efficiency from high order waveguide modes to Gaussian–like beams in free space, allowing them to be used in high power gyrotrons. QO launcher radiation pattern is simulated and optimized using Launcher Optimization Tool (LOT). The launcher parameters are given in Table 4.8. These parameters are optimized using LOT.

Table 4.8: Launcher Parameters.

Launcher Length	215	mm
Helical Cut Length	60	mm
Waveguide Radius	13.10	mm
Taper Angle	0.004	°

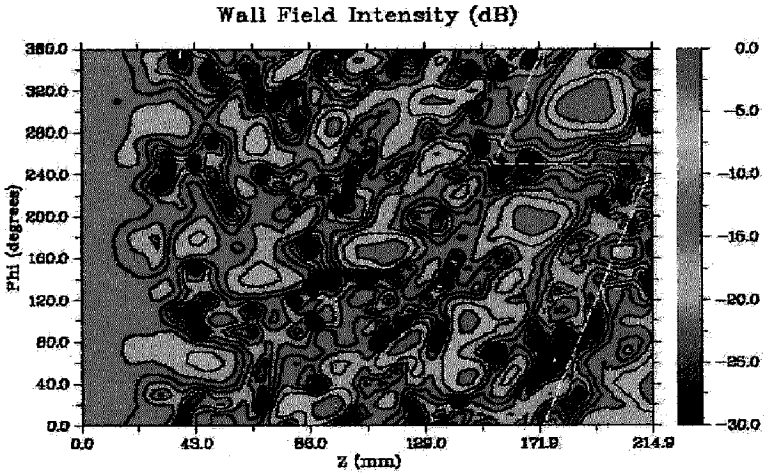

Figure 4.20: Wall Field Intensity of Launcher.

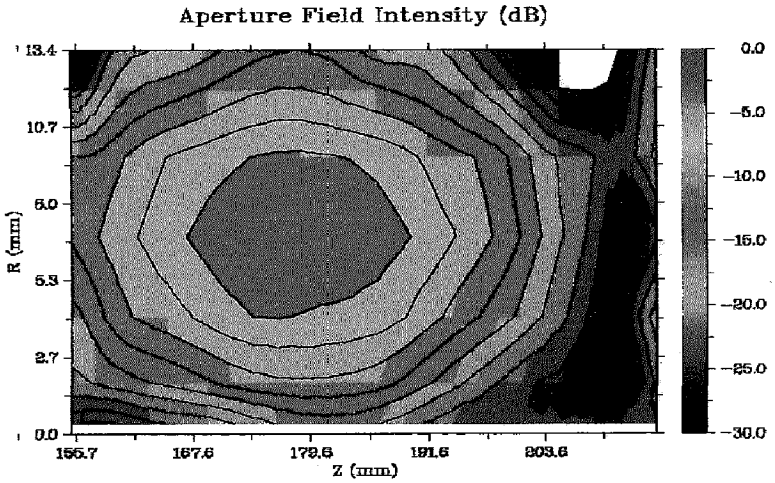

Figure 4.21: Aperture Field Intensity of Launcher.

The first step is to take only 2 sets of perturbations on type–2 surface (surface deformation points are calculated on the basis of the studies given by Hirata [30]) and optimize to get the maximum Gaussian fit. Then one more set of perturbation is included in the optimized file and again maximum Gaussian fit needs to be achieved. Same process is followed one more time to have four sets of perturbations in the same surface file on type–2 surface. Finally the surface is converted to type–3 surface using the surface converter and then optimized. The final Gaussian fit obtained using this design is 99.60 %. The wall field intensity and aperture field intensity obtained on type–3 surface after optimization using the Launcher Optimization Tool with four deformations are as shown in Fig. 4.20 and Fig. 4.21 respectively.

4.5.3 RF–Window

The RF–window is a critical component that transmits the output power to the external system. It must withstand high power, mechanical stresses, and pressure gradients. Therefore, care must be taken in selecting the proper window material with low–loss tangent, high thermal conductivity, and mechanical strength since the window must withstand large thermal and mechanical stresses. Ideally, it should also offer easy metallization/brazing and make a strong vacuum–tight seal with metals.

The state–of–the–art of window materials for high–power gyrotrons is described in [1, 45, 50]. For high–power CW gyrotrons at millimetric wavelengths, advanced materials such as sapphire, CVD diamond, Au–doped silicon, etc., have to be used. For the current conceptual design, a double disc window has been designed with sapphire as the window material. The window design is carried out for a Gaussian beam with radial output coupling with an estimated window aperture radius of 50 mm (approximately 1.67 times the Gaussian beam radius). The dimensions of both the disks are kept same. The design values are given in Table 4.9. The variation of the reflection and transmission with frequency for this design are as shown in

Fig. 4.22. A transmission of 98.127 % has been achieved for the design values in Table 4.9.

Table 4.9: Design values for Double disc Window.

Window material	Sapphire	
Window aperture radius (r_{dd})	50	mm
Disc thickness (D_1 and D_2)	2.447	mm
Distance between disks (t_{dd})	3.732	mm
Disc Dielectric Constant	9.41	
Loss Tangent of disc	5.56×10^{-5}	
Coolant Dielectric Constant	1.8	
Loss Tangent of coolant	26×10^{-4}	

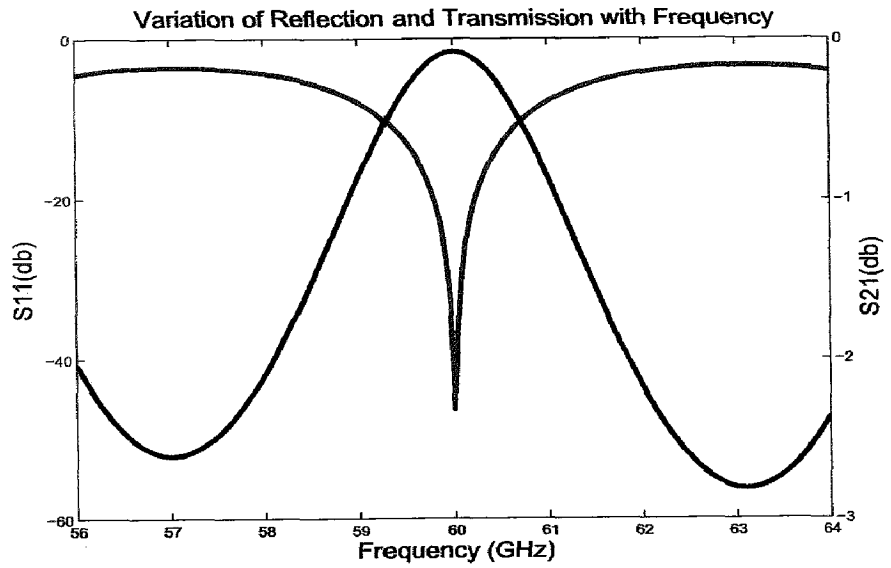

Figure 4.22: Transmission and Reflection Characteristics of the window.

4.5.4 Collector

After the interaction, the spent electron beam dissipates on the walls of the collecting surface. The magnetic field is reduced smoothly and sufficiently slowly towards the collector in a gyrotron so that the transverse momentum of the electrons decreases adiabatically. The uptapering of the output waveguide increases the collector area and thus reduces the power dissipation density at the collector surface, which is very important for operation at high average power levels. Conventionally, the installation of collector at an axial extent where the magnetic field reduces to ≈100 Gauss, gives satisfactory results.

For the current gyrotron, the magnetic field reduces from 2.32 T to 100 Gauss at a distance of 80 cm from the center of the cavity. The center of the cavity is at a distance of 338 mm from the electron gun and the point where magnetic field is 100 Gauss is at a distance of 1038 mm from the electron gun. So the axial extent of the collector is estimated to be around 80 cm to keep the average power density on its walls within the limit of 0.5 kW/cm^2. A first estimation of the collector position, its dimensions and its magnetic field requirements for sweeping purposes to lower the heat dissipation on the walls can be made by (i) observing the electron trajectories and/or magnetic field lines from the interaction, and (ii) noting the placement of the launcher and mirrors [16]. The design analysis of collector is carried out with electron trajectories obtained using ESRAY code. This design is beyond the purview of the thesis.

Chapter 5

Conclusions And Future Scope

5.1 Conclusions

The overall thesis work can be summarized as follows:

- The feasibility and conceptual design studies of CW operation of a 60 GHz conventional cavity gyrotron at a power > 100 kW have been presented in this thesis. The main application of this specific gyrotron is for plasma diagnostics in India. An efficiency of around 38% has been confirmed theoretically.

- The initial mode selection procedure has been carried out for 60 GHz. After the detailed study of mode competition through the starting current calculations $TE_{6,2}$ has been selected as the operating mode. Cold–cavity computations have been carried out to design the conventional cavity for this specific gyrotron. The output of these cold cavity calculations is further used in self–consistent computations to evaluate power and efficiencies. Finally the output system of the gyrotron has been designed which includes the non–linear taper, quasi–optical launcher and a double disc window.

- The triode type MIG has been designed using GDS code and optimized with the ESRAY code. The magnetic profile and other parameter values have been generated. The advanced dimpled–wall launcher has been designed using the

Launcher Optimization Tool.

- Gyrotron design software ***GDS V.01*** has been developed. It is a complete package which can be used for the design and conceptualization of specific gyrotrons. The calculations involved in the analysis of gyrotron operation can be performed. The initial design values required for the design of Magnetron Injection Gun and Quasi–optical Launcher can also be produced using this software. It also designs the non–linear taper and the RF window which can be either single disc or double disc. Suitable design plots are also generated in this software.

5.2 Future Scope

Some of the future works of the current research work are as follows:

- The design studies of the specific gyrotron can be used for plasma diagnostic applications. The more distant plans of gyrotron developers will be focused on the further escalation of the CW output power together with further enhancement of their efficiency and reliability.

- Also, the use of single–stage and multistage depressed collectors in such tubes operating with electron beams with more than 4–MW CW power are important future advances, as well as the related thermal management issues that include the intense cooling of large–diameter resonators and small–diameter inserts. All of these advances will simplify the microwave facility required for plasma experiments and substantially reduce its cost.

- The software *GDS* can be further developed to include some more features such as the inclusion of space charge effects and the time–dependent self consistent calculations. The design of the other variations of cavities, tapers and windows can also be included in the software.

Bibliography

[1] M. Thumm, "State-of-the-art of high power gyro-devices and free electron masers update 2009," Scientific Reports 7540, Karlsruhe Institute of Technology, Germany, April 2010.

[2] P. Woskoboinikow, "Development of gyrotrons for plasma diagnostics," *Review of Scientific Instruments*, March 1986.

[3] M. R. Siegrist, H. Bindslev, R. Brazis, D. Guyomarc'h, J. P. Hogge, Ph. Moreau and R. Raguotis, "Development of a high-power THz radiation source for plasma diagnostics," *Infrared Physics and Technology*, vol. 40, issue 3, pp. 247-259, June 1999.

[4] M.V. Kartikeyan, E. Borie, and M. Thumm, *Gyrotrons - High power microwave and millimeter wave technology*, Berlin-Heidelberg, Germany: Springer-Verlag, 2004.

[5] Y. Setsuhara, Y. Tabata, R. Ohnishi, S. Miyake, "Heating and sintering of alumina using high-power pulsed 60 GHz gyrotron," *Transactions of Joining and Welding Research Institute*, Osaka University, vol. 21, no. 2, 1992.

[6] H. Jory, S. Evans, K. Felch, J. Shively and S. Spang, "Gyrotron oscillators for fusion heating," in *Proceedings of the 3rd Joint Varenna - Grenoble International Symposium on Heating in Toroidal Plasmas*, Volume III, pp. 1073 - 1078, March 1982.

[7] J. S. Machuzak, P. P. Woskov, J. Gilmore, N. L. Bretz, H. K. Park, R. E. Aamodt, P. Y. Cheung, D. A. Russell, and H. Bindslev, "TFTR 60 GHz: Alpha particle collective thomson scattering diagnostic," in *Tenth Topical Conference on High Temperature Plasma Diagnostic Conference Rochester*, NY, 8-12 May, 1994.

[8] K. Felch. I. Bier. L. Fox, H. Huey, H. Jory, J. Manca, J. Shively, S. Spang, "Analysis of the output mode from 60 GHz, 200 kW pulsed and CW gtrotrons, in *8th International Conference on Infrared and Millimeter Waves*, Miami Beach, 12 Dec. 1983.

[9] K.L. Felch, B.G. Danly, H.R. Jory, K.E. Kreischer, W. Lawson, B. Levush, R.J. Temkin, "Characteristics and applications of fast-wave gyrodevices," *Proceedings Of The IEEE*, vol. 87, no. 5, pp. 752-781, May 1999.

[10] K.R. Chu, "The electron cyclotron maser," *Reviews of Modern Physics*, vol. 76, no. 2, pp. 489-540, 2004.

[11] A.G. Litvak, "High power gyrotrons. Development and applications," in *33rd International Conference on Infrared, Millimeter and Terahertz Waves*, pp. 1-4, 15-19 Sep. 2008.

[12] G. S. Nusinovich, *Introduction to the physics of gyrotrons*, Baltimore and London: The Johns Hopkins University Press, 2004.

[13] M. Thumm, "High-power Gyro-devices for plasma heating and other applications," *International Journal of Infrared and Millimeter Waves*, vol. 26, no. 4, pp. 483-503, April 2005.

[14] M. Thumm, "Progress in gyrotron development," *Fusion Engineering and Design*, vol. 66-68, pp. 69-90, Sep. 2003.

[15] M. Thumm, "Progress in the development of high-power millimeter- and submillimeter wave gyrotrons and of free electron masers," *Archiv fur Etektrotechnik*, Springer-Verlag, vol.77, pp. 51- 55, 1994.

[16] M.V. Kartikeyan, E. Borie, B. Piosczyk, O. S. Lamba, V. V. P. Singh, A. Mobius, H. N. Bandopadhyay, and M. Thumm, "Conceptual design of a 42 GHz, 200 kW gyrotron operating in the $TE_{5,2}$ mode," *International Journal of Electronics*, vol. 87, pp. 709–723, 2000.

[17] A. V. Gaponov, V. A. Flyagin, A. L. Gol'denberg, G. S. Nusinovich, S. E. Tsimring, V. G. Usov, and S. N. Vlasov, "Powerful millimeter-wave gyrotrons," *International Journal of Electronics*, vol. 51, pp. 277, 1981.

[18] M. V. Kartikeyan, E. Borie, O. Drumm, B. Piosczyk, and M. Thumm, "Design of a 42 GHz, 200 kW gyrotron operating at the second harmonic," *IEEE Transactions on Microwave Theory and Techniques*, vol. 52, no. 2, pp. 686-692, Feb. 2004.

[19] G. Gantenbein and E. Borie, "Gyrotron with a tapered external magnetic field," *International Journal of Infrared and Millimeter Waves*, vol. 11, no. 7, pp. 837-850, 1990.

[20] S.N. Vlasov, G.M. Zhislin, I.M. Orlova, M.I. Petelin, G.G. Rogacheva, "Irregular waveguides as open resonators," *Radiophysics Quantum Electronics*, vol. 12, pp. 972-978, 1969.

[21] V.L. Bratman, M.A. Moiseev, M.I. Petelin, "Theory of gyrotrons with low- Q electromagnetic systems," from 'Gyrotrons: collected papers', USSR Academy of Sciences, Insitute of Applied Physics, Gorki, 1981.

[22] I.G. Zarnitsina, G.S. Nusinovich, "Competition between modes resonant with different harmonics of the cyclotron frequency in gyromonotrons," *Radiophysics Quantum Electronics*, vol. 20, pp. 461-467, 1977.

[23] E.Borie, *Gyrotron oscillators : Their principles and practice*, edited by C. J. Edgcombe (Taylor & Francis, London, 1993), Ch. 3.

[24] A.W. Fliflet, M.E. Read, K.R. Chu, and R. Seeley, "A self-consistent field theory for gyrotron oscillators: application to a low Q gyromonotron," *International Journal of Electronics*, vol. 53, pp. 505-521, 1982.

[25] K.E. Kreischer, B.G. Danly, J.B. Schutkeker, R.J. Temkin, "The design of megawatt gyrotrons,", in *IEEE Transactions on Plasma Science PS-13*, pp. 364-373, 1985.

[26] M. Thumm, "Present developments and status of electron sources for high power gyrotron tubes and free electron masers," *Applied Surface Science*, vol. 111, pp. 106-120, 1997.

[27] V.L. Granatstein, B. Levush, B.G. Danly, R.K. Parker, "A quarter century of gyrotron research and development," *IEEE Transactions on Plasma Science*, vol.25, no.6, pp.1322-1335, Dec.1997.

[28] D. Wagner, M. Thumm, G. Gantenbein, W. Kasperek, and T. Idehara, "Analysis of a complete gyrotrons oscillator using the scattering matrix description," *International Journal of Infrared Millimeter Waves*, vol. 19, no. 2, pp. 185-194, 1998.

[29] Y. Hirata, Y. Mitsunaka, K. Hayashi, Y. Itoh, K. Sakamoto and T. Imai, "The design of a tapered dimple-type mode converter/launcher for high-power gyrotrons," *IEEE Transactions on Plasma Science*, vol. 31, no. 1, pp. 142-145, Feb. 2003.

[30] J. Jin, B. Piosczyk, M. Thumm, T. Rzesnicki, and S. Zhang, "Quasi-optical mode converter/mirror system for a high power coaxial-cavity gyrotron," *IEEE Transactions on Plasma Science*, vol. 34, no. 4, pp. 1508-1515, Aug. 2006.

[31] J. Jin, "Quasi-optical mode converter for a coaxial cavity gyrotron," Wissenschaftliche Berichte, FZKA 7264, Karlsruhe, March 2007.

[32] M. Thumm, "Quasi-optical gyrotron mode converters," in *Colloquium on Gyrotrons, 6th Greek School on Fusion Physics and Technology*, University of Thessaly, Volos, Greece, 26–31 March 2007.

[33] R.A. Olstad, J.L. Doane, C.P. Moeller, R.C. O'Neill, M. DiMartino, "High-power corrugated waveguide components for mm-wave fusion heating systems," in *19th Symposium on Fusion Technology*, Lisbon, Portugal, 16-20 Sep. 1996.

[34] G.G. Denisov, V.E. Zapevalov, A.G. Litvak, and V.E. Myasnikov, "Megawatt gyrotrons for ecr heating and current-drive systems in controlled-fusion facilities," *Radiophysics and Quantum Electronics*, vol. 46, no. 10, pp. 757-768, 2003.

[35] T.V. George, "High average power microwave sources for fusion research," in *International Vacuum Electronics Conference*, Abstracts, pp. 1-2(18.1), May 2000.

[36] K. Sakamoto, "Major improvement of gyrotron efficiency with beam energy recovery," *Physical Review Letters*, vol. 73, no. 26, pp. 3532-3535, 1994.

[37] M. Morozkin, G. Denisov, M. Glyavin, A. Luchinin, M. Petelin, D. Sobolev, "Development of high efficient technological gyrotron with depressed collector," in *The 6th International Kharkov Symposium on Physics & Engineering of Microwaves, Millimeter and Sub-millimeter Waves and Workshop on Terahertz Technologies*, vol. 2, pp. 571-573, 25-30 June 2007.

[38] J. M. Baird and W. Lawson, "Magnetron injection gun (MIG) design for gyrotron applications," *International Journal of Electronics*, vol. 61, pp. 969–984, 1986.

[39] Stefan Illy, "*ESRAY– A computer code for the analysis of axisymmetric electron guns*," Private communication, 2002.

[40] J.R.M. Vaughan, "Representation of axisymmetric magnetic fields in computer programs," *IEEE Transactions on Electron Devices*, vol. 19, pp. 144, 1972.

[41] A.W. Fliflet and M.E. Read, "Use of weakly irregular waveguide theory to calculate eigenfrequencies, Q-values and RF field functions for gyrotron oscillators," *International Journal of Electronics*, vol. 51, pp. 475–484, 1981.

[42] E. Borie and O. Dumbrajs, "Calculation of eigenmodes of tapered gyrotron resonators," *International Journal of Electronics*, vol. 60, pp. 143–154, 1986.

[43] E. Borie, B. Jodicke, and O. Dumbrajs, "Self consistent code for a 150 GHz gyrotron," *International Journal of Electronics*, vol. 7, pp. 1863–1879, 1986.

[44] *Launcher Optimization Tool*, User Manual, Version 1.21, Calabazas Creek Research, Inc., 2006.

[45] H.-U. Nickel, "Aspects of high frequency technology for the development of low-reflection output windows for high power millimeter-wave gyrotrons," Forschungszentrum Karlsruhe, Karlsruhe, Germany, Scientific Report FZKA 5513, 1995.

[46] S. Kern, "Numerische Simulation der Gyrotron-Wechselwirkung in koaxialen Resonatoren," Forschungszentrum Karlsruhe, Scientific Report, FZKA 5837, Nov. 1996.

[47] W. G. Lawson, "Theoretical evaluation of non-linear tapers for a high power gyrotrons," *IEEE Transactions on Microwave Theory and Techniques*, vol. 38, no. 11, pp. 1617-1622, 1990.

[48] N. Chauhan, A. Mittal, D.Wagner, M.V. Kartikeyan, M. Thumm, "Design and optimization of nonlinear tapers using particle swarm optimization," *Interna-*

tional Journal of Infrared & Millimeter Waves, vol. 29, no. 8, pp. 792-798, August 2008.

[49] Jeffrey M. Neilson, "Optimal synthesis of quasi-optical launchers for high-power gyrotrons," *IEEE Transactions on Plasma Science*, vol. 34, no. 3, pp. 635-641, June 2006.

[50] M. Thumm, "Development of output windows for high power long pulse gyrotrons and EC wave applications," *International Journal of Infrared Millimeter Waves*, vol. 19, pp. 3-14, 1998.

List of Publications

1. **Ragini Jain**, J. C. Mudiganti, and M. V. Kartikeyan,"Mode Selection for 60 GHz, 100 kW CW Gyrotron for Plasma Diagnostics," in *Indian Vacuum Society National Symposium (IVSNS-09)*, CEERI Pilani, India, Nov 2009.

2. **Ragini Jain**, and M. V. Kartikeyan,"Mode Competition and Cavity Design Studies of a 60 GHz, 100 kW, CW Gyrotron," in *National Conference on Advances in Microwave Communication, Devices and Applications*, Jaipur, India, Feb 2010.

3. **Ragini Jain**, M. V. Kartikeyan,"Design studies of a 100 kW, 60 GHz CW Gyrotron for Plasma Diagnostics," in *The 35th International Conference on Infrared, Millimeter and Terahertz Waves 2010*, Rome, Italy, Sep 2010 (Accepted).

4. **Ragini Jain**, and M. V. Kartikeyan,"Design of a 60 GHz, 100 kW CW Gyrotron for Plasma Diagnostics: GDS-V.01 Simulations," Communicated to *Progress In Electromagnetics Research*, June 2010.